ELSEVIER

Colloids and Surfaces
A: Physicochemical and Engineering Aspects 187–188 (2001) 539–568

COLLOIDS AND SURFACES A

www.elsevier.nl/locate/colsurfa

Review

Water in porous carbons

John K. Brennan [a,*], Teresa J. Bandosz [b], Kendall T. Thomson [c], Keith E. Gubbins [a]

[a] *Department of Chemical Engineering, North Carolina State University, Raleigh, NC 27695-7905, USA*
[b] *Department of Chemistry, City College of New York, New York, NY 10031, USA*
[c] *School of Chemical Engineering, Purdue University, West Lafayette, IN 47907-1283, USA*

Abstract

We present an overview of progress in understanding the behavior of water in porous carbons at the molecular level. We survey experimental investigations, semi-empirical approaches, and simulation studies. Experimental work faces a number of challenges: the determination of the distribution of carbon microcrystal sizes, the densities and species of surface groups, the topological nature of the connected pore structure, and pore size distributions. The lack of experimental characterization, together with the uncertainty in the intermolecular potentials involved, has thwarted molecular simulation efforts thus far. A concerted approach that links experimental and simulation efforts appears promising in gaining a better understanding of the behavior of water in porous carbons. Experimental results could aid in the development of realistic carbon models and improve the intermolecular potentials used in the simulation studies. In a complementary fashion, molecular simulation could help improve characterization methods of both the carbon structure and the surface chemistry.

Keywords: Water; Activated carbons; Adsorption; Molecular modeling; Molecular simulation

1. Introduction

Activated carbons are the most widely used industrial adsorbent for removing contaminants and pollutants from gaseous, aqueous and non-aqueous streams, due in part to their uniquely powerful adsorption properties and the ability to readily modify their surface chemistry. They are also widely used as electrode materials in fuel cells, as catalyst supports, and as fibers for structural reinforcement in composites or filters. The presence of water in graphitic and activated carbons can severely handicap the intended process. For example, quite low humidities in gases entering industrial adsorbers are known to have a large effect on the capacity and selectivity for the removal of organic and inorganic contaminants (see, e.g. Ref. [1]). Similarly, small amounts of water often reduce the diffusion rates of alkanes in microporous media by an order of magnitude

* Corresponding author. Tel.: +1-919-513-2051; fax: +1-919-513-2470.
E-mail address: jbrennan@unity.nscu.edu (J.K. Brennan).

0927-7757/01/$ - see front matter
PII: S0927-7757(01)00644-6

[2]. The mechanism producing these effects is poorly understood.

The adsorption of water on activated carbons is quite different from that of non-associating simple fluids, such as nitrogen, carbon dioxide, or hydrocarbons [3]. The main underlying differences stem from the strong water–water interactions, the weak water–carbon interactions, and the formation of hydrogen bonds with oxygenated groups on the surface. Therefore, our understanding of the behavior of simple fluids in confinement cannot be applied to water in porous carbons.

Progress in understanding the behavior of water in activated carbons at a molecular level has been slow for several reasons. Activated carbons are derived from a wide variety of precursors, and thus their amorphous pore structure has proved to be among the most difficult to characterize. Experimental characterization of these materials faces a number of challenges, including, determining (a) the distribution of carbon microcrystal sizes; (b) the densities and species of surface groups; (c) the topological nature of the connected pore structure; and (d) pore size distributions. The details of pore filling are sensitive to the size and arrangement of graphite microcrystals, the pore size distribution, the species and arrangement of the surface groups, etc. Little is known of the effect of these variables on phase changes (e.g. capillary condensation and freezing) for confined water, although these transitions are known to be strongly dependent on the species and density of the surface sites. The molecular role played by water adsorption in mixtures is also poorly understood.

The lack of experimental characterization, together with the uncertainty in the intermolecular potentials involved, have thwarted molecular simulation efforts thus far. A coordinated approach that links experimental and simulation efforts appears promising in gaining a better understanding of the behavior of water in porous carbons. Experimental results could aid in the development of realistic carbon models and improve the intermolecular potentials used in the simulation studies. In a complementary fashion, simulation could help improve characterization methods of both the carbon structure and the surface chemistry. Improved characterization of the activated carbons and further understanding of the adsorption mechanism can only come from a joint effort that combines structural investigations (neutron scattering, small angle X-ray scattering (SAXS), TEM), surface characterizations (Fourier transform infrared spectroscopy (FTIR), X-ray photoelectron spectroscopy (XPS), Boehm and potentiometric titration), and adsorption studies (adsorption isotherms, isosteric heats) with molecular simulations based on realistic models.

In this paper, we present an overview of recent progress in understanding the behavior of water in porous carbons at the molecular level. We survey experimental investigations, semi-empirical approaches, and simulation studies. In Section 2, we review experimental works. The classical, semi-empirical methods of correlation are discussed in Section 3. Next (Section 4) we explore methodologies for modeling realistic carbon structures. We also review the current state of intermolecular potential models for water and oxygenated sites on the carbon surface. Finally (Section 5), we give an overview of the molecular simulation work that has been done on the adsorption of water in microporous carbons.

2. Experimental studies

In this section, we present an overview of experimental investigations of the behavior of water in porous carbons. First, we provide an overall description of the adsorption behavior, followed by a review of studies to characterize the surface chemistry of activated carbons.

2.1. Adsorption behavior

Although many papers have been published describing the behavior of water–carbon systems, there is a lack of consensus in understanding the mechanism of the adsorption and in explaining the shape of the resulting isotherms [4–43]. Several predictive models have been proposed; unfortunately all of them have failed to satisfactorily describe the isotherms over the entire relative-pressure range P/P_0, (where P_0 is the bulk fluid saturation pressure) [4–8,11,16,19].

The isotherms of water adsorption differ significantly from the adsorption of organic compounds. This is illustrated in Fig. 1, where adsorption isotherms for *n*-hexane and water on graphitized carbon black are shown. For *n*-hexane the dispersion interaction with the carbon atoms is strong, leading to significant adsorption at low pressure, followed by a buildup of further adsorbed layers as pressure is increased. By contrast, the adsorption of water is essentially zero for $P/P_0 < 0.7$, and remains small up to $P/P_0 = 1.0$. The dispersion interaction for water is small. More importantly, the adsorption behavior is determined by the ratio of the fluid–wall attractive interaction to the fluid–fluid attractive interaction [44]. For water this ratio is very small, due to the strong hydrogen bonding (H-bonding) between water molecules. Graphitized carbon does not have an appreciable number of surface groups for water to H-bond to.

For porous carbons having some oxygenated surface groups, the most commonly reported isotherms are of IUPAC classification Type V (S-shape), where sorption at low relative-pressure is negligible and a significant uptake occurs at higher pressure (usually at P/P_0 around 0.5). Another common feature of such water isotherms is a hysteresis loop that increases with increased burn-off of carbon [4]. Examples of such isotherms are shown in Fig. 2. These isotherm shapes are a consequence of the hydrophobic nature of the activated carbon surface. When the density of polar groups on the carbon surface are reduced, thus decreasing the surface hydrophobicity, the isotherms change shape and are classified as Type IV [11,20], Type III [22,23], or Type II [24]. The density of polar groups on the surface can be controlled by heating the carbon in a reducing atmosphere (thus decreasing the surface density of groups) or an oxidizing one (to increase

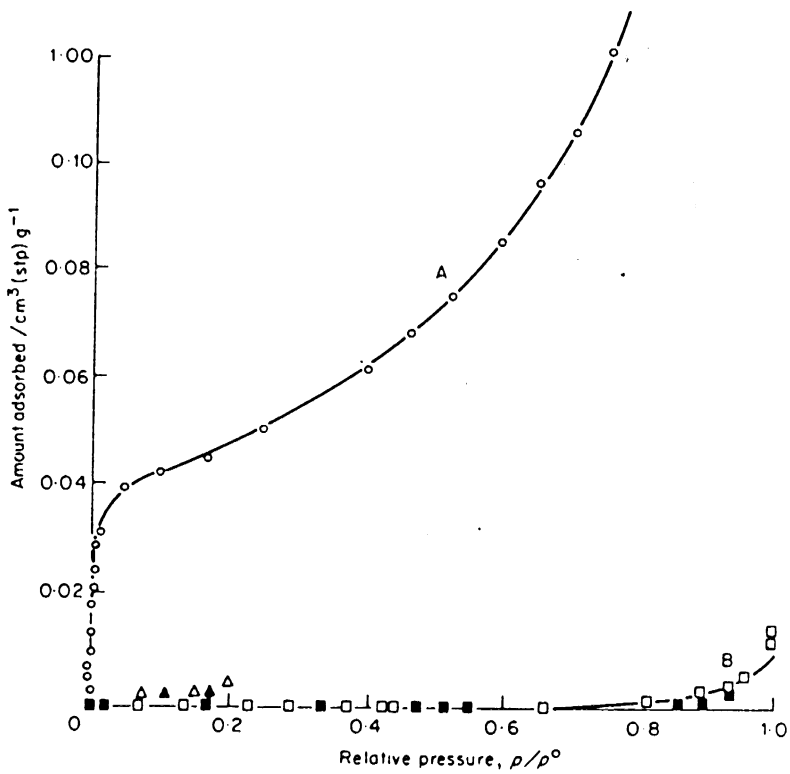

Fig. 1. The adsorption isotherms of *n*-hexane (A) and of water (B) on graphitized carbon black [3]. Solid symbols denote desorption. Reprinted from Ref. [3] with permission from Academic Press.

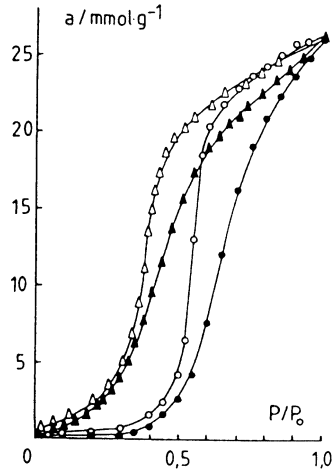

Fig. 2. The adsorption of water by samples 1 (circles) and 2 (triangles) at 293 K, containing, respectively, 4.6 and 26.5% of primary centers. Open symbols refer to desorption data. Reprinted from Ref. [27] with permission from Elsevier Science.

group density). Some examples of experimental isotherms for different types of carbons treated in this way are presented in Figs. 3 and 4. The differences in the shape of the isotherms in these figures are the result of the combined effects of

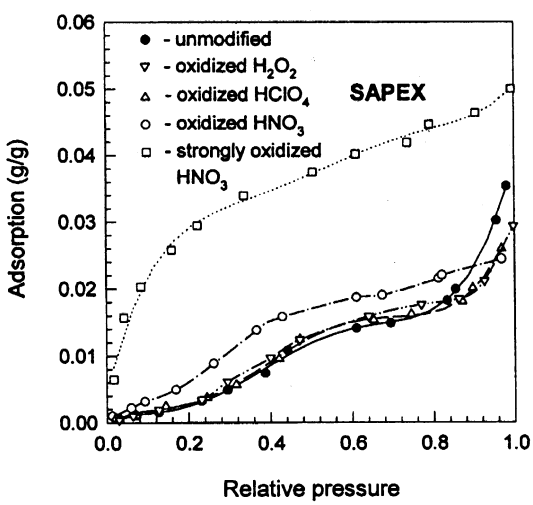

Fig. 3. Adsorption isotherms for water vapor on SAPEX carbon black samples, before and after oxidation using various reagents. Reprinted from Ref. [21] with permission from the Journal of Colloids and Interface Science.

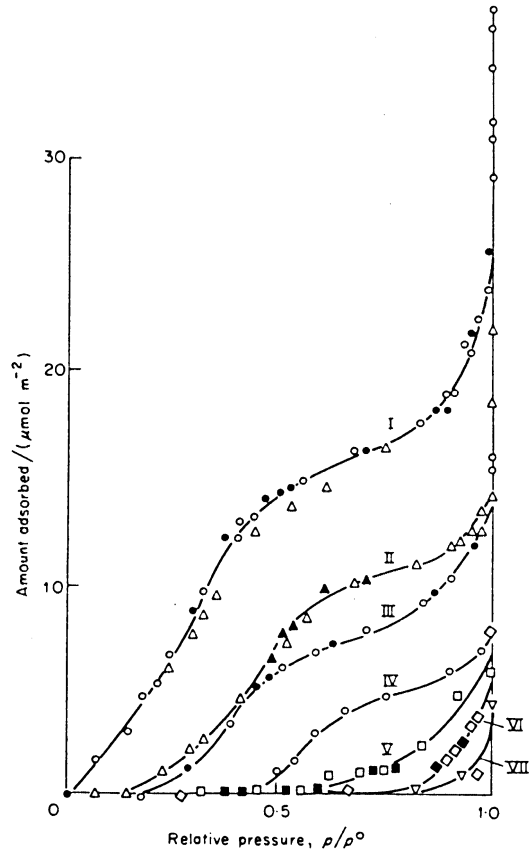

Fig. 4. Adsorption of water vapor on oxygenated carbons: (I) heated in vacuo at 200°C; (II) in vacuo at 950°C; (III) in vacuo at 1000°C; (IV) at 1100°C in a hydrogen stream; (V) in hydrogen at 1150°C; (VI) in hydrogen at 1700°C; and (VII) at 3200°C. Reprinted from Ref. [13] with permission from Academic Press.

carbon hydrophobicity and the presence of surface functional groups that act as primary adsorption centers. It is believed that water molecules are adsorbed strongly on the surface sites via H-bonding. This is followed by further adsorption that results in the creation of water clusters, and eventual pore filling. When the density of groups is relatively high, a Type II isotherm is obtained. In contrast, for carbons having no surface groups (graphitic carbon), a Type III (non-porous carbons) or Type V (porous carbons) isotherm is expected. For graphitic carbons, at low pressure the adsorption is negligible while capillary condensation occurs at about $P/P_0 \sim 0.5$. These find-

ings have lead to a few widely accepted generalizations of the mechanism of water adsorption which includes the following steps: (1) the adsorption of water on surface functional groups; (2) the adsorption of water on previously adsorbed water molecules and subsequent cluster formation; (3) pore filling occurs at about $P/P_0 = 0.5$; and (4) a plateau is reached at high pressure when all pores are filled.

A closer look at the isotherms measured at very low pressure reveals more information about the adsorption process and cluster formation. Adsorption isotherms obtained for carbons having varying densities of oxygenated groups showed that at very low pressure the general shape of the isotherms is similar, regardless of the type of carbons [12,37,38]. Such behavior is illustrated in Fig. 5 for a single carbon sample. This behavior has been found to be consistent at different temperatures.

When adsorption experiments are carried out at various temperatures one can calculate the isosteric heats of adsorption (Q_{st}) from the Clapeyron equation, provided that the process is reversible and that adsorption equilibrium is achieved [12,37,41,43]. When Q_{st} is calculated from isotherms for which the first measured point is at $P/P_0 \sim 0.1$, Q_{st} was found to have values very close to the latent heat of bulk water condensation, 45 kJ mol^{-1} [29,30,39]. This finding indicates that the formation of water clusters around primary sites must occur at very low relative-pressure, below $P/P_0 \sim 0.1$, so that subsequent adsorption is with pre-adsorbed water molecules.

The low surface coverage regime has been reached using chromatographic techniques, and the heat of water adsorption reported for nonporous carbon black (assuming a monolayer of adsorbed water) was about 20 kJ mol^{-1} [31]. This low value (much lower than the heat of condensation) is consistent with the low affinity of the graphene surface towards the water molecule. Similar values calculated from carefully measured isotherms in the pressure range from 1 to 3 Torr was reported by Naono et al. [41] on hydrophobic microporous activated carbons. Their surface coverage was higher by 0.02 molecules nm^{-2} than that for the carbon used in Ref. [31], and the heat showed an increasing trend with adsorption coverage, from 15 to 32 kJ mol^{-1} depending on the type of carbon (Fig. 6). The authors suggested that the trend was due to an increase of energy from more water–water interactions. Salame and Bandosz observed a similar trend in the heat of

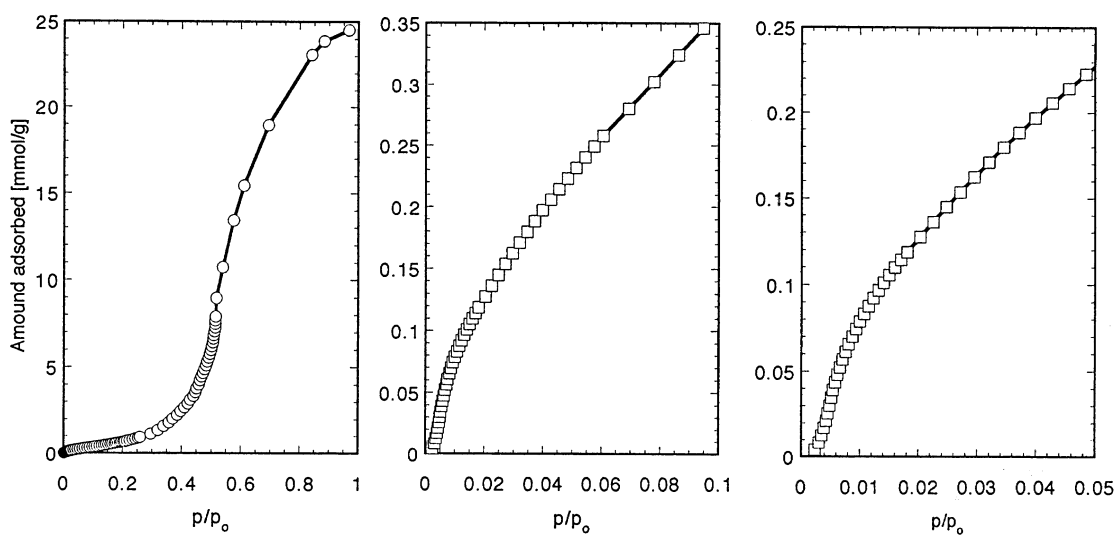

Fig. 5. Examples of water adsorption isotherms on activated carbons for the full pressure range up to $P/P_0 = 1$ (figure at left) and at low pressure (center and right figures).

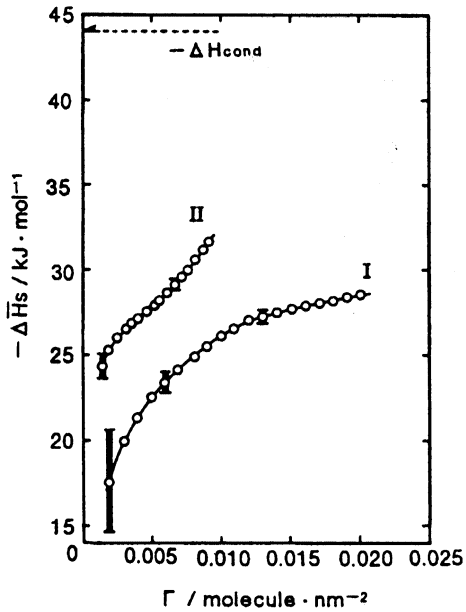

Fig. 6. Differential enthalpy of adsorption ($-\Delta H_s$) of water vapor for high surface area activated carbon (I: AC-1) and activated carbon fiber (II: AC-2). Reprinted from Ref. [41] with permission from the Journal of Colloids and Interface Science.

adsorption on various activated carbons with different degrees of surface oxidation [12,37,38,43], as shown in Fig. 7. However, in that study the heat of condensation of bulk water was reached at a relatively low surface coverage (less than 1

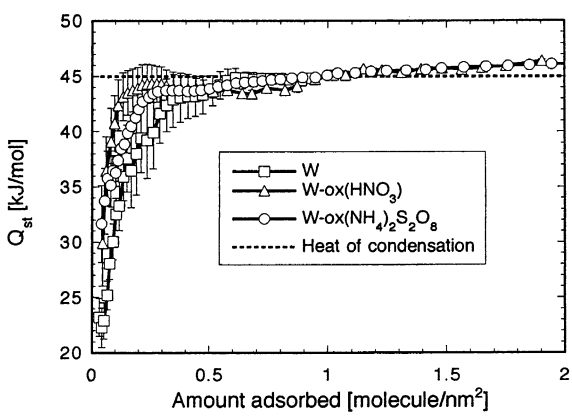

Fig. 7. Isosteric heats of water adsorption on initial and oxidized carbons. The horizontal dashed line is the latent heat of condensation of bulk water.

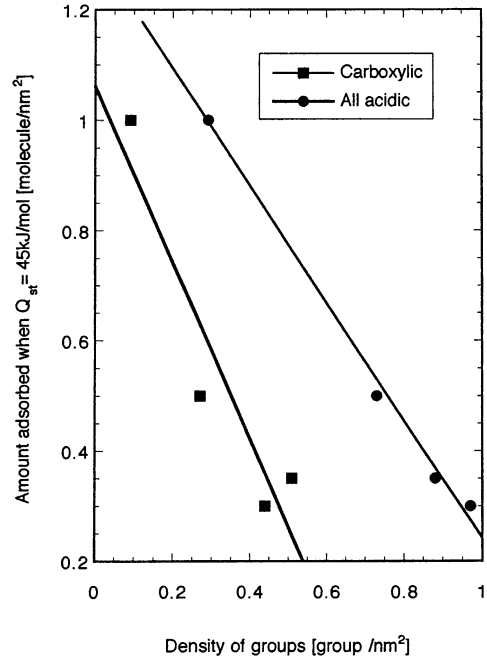

Fig. 8. Dependence of the amount of water adsorption at which the isosteric heat becomes equal to the bulk heat of condensation on the density of carboxylic and acidic groups of one series of activated carbons.

molecule nm^{-2}). The coverage at which the heat of adsorption was equal to the heat of condensation was directly proportional to the number of surface oxygen groups. Additionally, surface oxygen groups with carboxylic sites were found to be the strongest adsorption centers (Fig. 8). The initial values of the heat were higher (by ~ 30 kJ mol^{-1}) for strongly oxidized carbons compared to materials with less severe oxidative treatment. For carbons with a low density of groups, the initial reported heat was between 17 and 20 kJ mol^{-1}. The steep rise exhibited in the plot of the dependence of the heat on coverage for oxidized carbon suggests rapid cluster formation. This results in an increased heat due to the increasing contribution of H-bonds. The H-bond energy for water with surface groups should be about 10–14 kJ mol^{-1}, so that the observed trend is consistent with the mechanism of the physical adsorption process and cluster formation [14].

It was found that pore size plays a significant role in the observed energetics of the adsorption

process [12,43]. In small pores, bridging between clusters occurs at very low pressure and the released heat of condensation makes any further heat effect insensitive to surface chemistry or porosity. It was also found that when pores are too small to accommodate functional groups, the released heat at very low relative-pressure is equal to the heat of condensation and has even been observed to be a few kiloJoules per mole above the heat of condensation [43]. This is consistent with the findings of Kaneko and coworkers [9,10] who studied the adsorption of water in molecular sieving carbons. Based on X-ray diffraction of the adsorbed water molecules, they concluded that water forms an ordered assembly structure in the hydrophobic nanospace. The estimated size of such a cluster is about 0.6 nm, and is likely associated with the macroscopic anomalies of water confined in a small pore. If such a structure exists, it may result in a release of heat equal to the heat of condensation at very low relative-pressure. When the cluster is located in pores equal to its size, it may also slightly enhance the adsorption energy due to dispersive interactions with the pore walls.

An increasing trend in the differential heat of water adsorption on non-porous carbon adsorbents with varying number and density of primary adsorption centers was also reported by Vartapetyan et al. [40]. They found that the heat of immersion increases with an increasing amount of pre-adsorbed water up to the maximum adsorption, implying that the differential heat of adsorption is lower than the heat of condensation over the entire range of filling. The recorded heat started at about 10 $kJ\,mol^{-1}$ and reached the heat of condensation for an adsorption of ~ 4 $\mu mol\,g^{-1}$. Results obtained for these non-porous carbons found only 40% of the surface occupied by clusters at the saturation pressure because distances between neighboring clusters were bigger than their diameters. The clusters that formed consisted of about 150 molecules per primary adsorption center and had an estimated diameter of about 3 nm. For carbons with a distance between sites smaller than the size of the cluster, a continuous film of water was created [40].

Based on the observed behavior outlined above, significant differences exist in the adsorption mechanism of water compared to simple fluids. The typical adsorption behavior of simple fluids on heterogeneous solids is not observed because the water–graphite interaction energy is very low [1] and the energy of H-bonding is relatively high [31]. When larger pores contribute to the adsorption process, a high initial heat (which is a consequence of enhanced adsorption energy in small pores) followed by a decrease in the heat of adsorption is not observed. On the contrary, an increase in the heat of adsorption is noticed due to increasing contributions of H-bonding between functional groups and other water molecules. The observation that the heat of adsorption equals the heat of water condensation results directly from cluster formation. This phenomenon occurs at a much lower pressure than the steep rise behavior exhibited in the isotherm (at $P/P_0 \sim 0.5$), which is a result of pore filling. The experimental results suggest that the smallest pores are filled first due to the cluster formation whereas larger pores require more water to create enough clusters to ensure complete pore filling.

In general, authors of the experimental works described above agree with the mechanism of adsorption via cluster formation followed by micropore filling. However, significant discrepancies exist between: (i) the detailed description of how the micropores are filled; (ii) the role of specific surface groups and their energy of interaction with water molecules; (iii) a quantitative description of the isotherms that is universal for all carbons with low and high densities of surface groups; and (iv) for the process over the entire relative-pressure range. Molecular modeling and simulation studies may prove fruitful in resolving some of these discrepancies.

2.2. Surface chemistry

To accurately model activated carbon–water interactions, the 'real' surface of the adsorbent has to be considered from both qualitative and quantitative points of view. It is well known that activated carbons or carbon fibers are not comprised of pure graphene layers. Among atoms

other than carbon that are present in the structure, the most common are hydrogen, oxygen, nitrogen, phosphorus, and sulfur [45–47]. They are incorporated in the aromatic rings as heteroatoms or present in the form of functional groups analogous to those classified in organic chemistry (see Fig. 9). It is believed that these groups are located at the edges of the graphene layers. Their presence results in surface chemical heterogeneity caused mainly by differences in the electronegativity of the heteroatoms relative to the carbon atoms. Groups such as OH, NH_2, OR, or O(C=O)R are classified as electron donors (due to the presence of σ or π electrons), whereas (C=O)OH, (C=O)H, or NO_2 groups are classified as electron acceptors (due to the presence of empty orbitals). Another classification is based on the strength of Brønsted acids. Their effective strength is described using the acid dissociation constant, pK_a. For example, most carboxylic acids have a pK_a between 2 and 6 and most phenols between 8 and 10 [48,49]. The main cause for carbon basicity is the absence of oxygen-containing groups at the edges of the crystallites [50]. Oxygen-containing groups, such as chromene and pyrone-type, also contribute to the basic character of activated carbon surfaces [47–49].

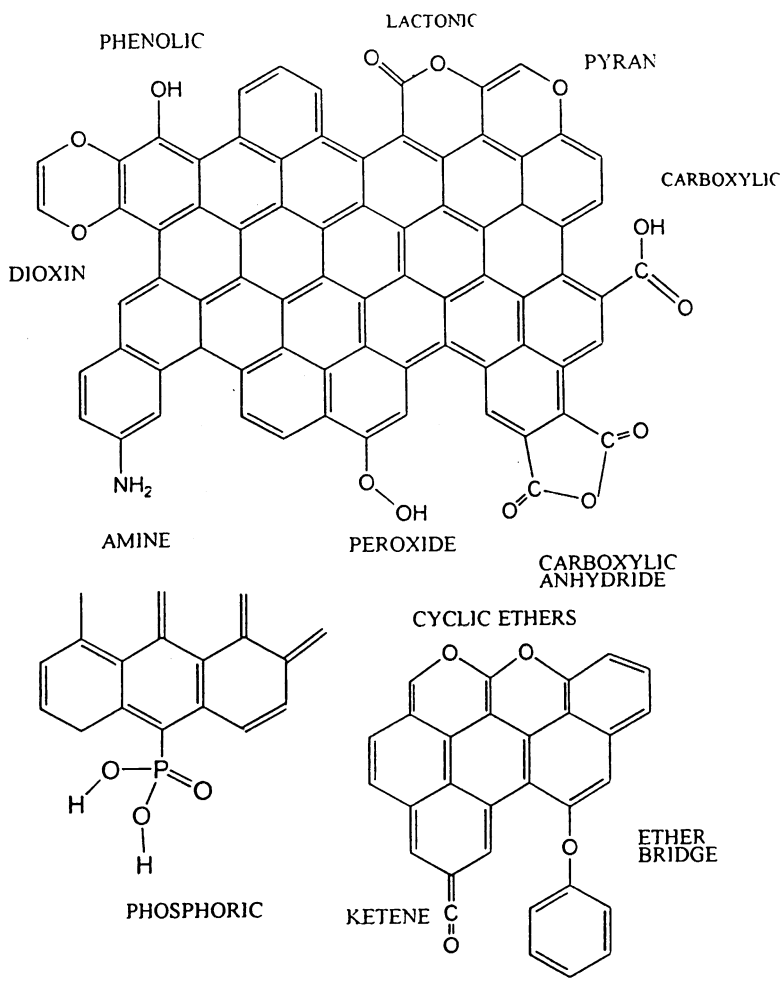

Fig. 9. Carbon surface chemistry. Heteroatoms and groups commonly found in activated carbons.

The simplest and most often used method to evaluate the quality and quantity of carbon surface groups was proposed by Boehm [46]. In this approach, a base of a certain strength neutralizes only acids having a pK_a smaller than or equal to that of the base. Typical bases used are: sodium bicarbonate, $NaHCO_3$ ($pK_a = 6.37$); sodium carbonate, Na_2CO_3 ($pK_a = 10.25$); sodium hydroxide, NaOH ($pK_a = 15.74$); and sodium ethoxide, $NaOC_2H_5$ ($pK_a = 20.58$). It is assumed that sodium bicarbonate neutralizes carboxylic acids; sodium carbonate neutralizes both carboxylic acids and lactones; sodium hydroxide neutralizes carboxylic acids, lactones, and phenols; whereas sodium ethoxide will react with all oxygen species, even extremely weak acids ($pK_a < 20.58$). The supplement to Boehm titration using bases is the determination of surface basic groups by titration with hydrochloric acid [51].

The other method that exploits acid–base interactions is *potentiometric titration* [52–57]. In this approach it is assumed that the system consists of acidic sites characterized by their acidity constants, pK_a. It is also assumed that the population of sites can be described by a continuous pK_a distribution, $f(pK_a)$. The experimental data can be transformed into a proton binding isotherm, Q, representing the total amount of protonated sites which is related to the pK_a distribution by the following integral equation:

$$Q(\mathrm{pH}) = \int_{-\infty}^{\infty} q(\mathrm{pH},pK_a)f(pK_a)\,\mathrm{d}pK_a \qquad (1)$$

After solving the above equation [58], the distribution of the surface pK_a is obtained in the experimental window for $pK_a = 3$–11. For very heterogeneous surfaces, many peaks are present [19,53–55]. The number of groups evaluated from potentiometric titration is in agreement with the Boehm method. However, more detailed information is obtained [56,57].

Temperature-programmed desorption (TPD), or thermodesorption, has been developed to evaluate the active surface area (ASA) of carbons [59]. Upon heating, the surface groups decompose, thereby releasing CO, CO_2, water, and hydrogen. The most acidic groups (carboxyls and lactones) are desorbed as CO_2 in the temperature range of 200–650°C, while less acidic (phenols and carbonyls) and basic (pyrones) groups are desorbed mainly as CO or $CO + CO_2$ in the temperature range of 500–1000°C [60,61]. The presence of water is a result of the decomposition of carboxylic groups.

Besides the methods presented above, XPS has been extensively used to describe the surface chemistry of carbon blacks, activated carbons, and carbon fibers [62–64]. The analysis is based on the changes of the intensities of 1s peaks of carbon, oxygen, or other heteroatoms, such as nitrogen. Those peaks are at specific irradiation energies related to the binding energies of core electrons ejected from atoms located on the external surfaces. The identification of oxygen functional groups is based on the analysis of the deconvoluted O_{1s} and C_{1s} peaks. The interpretation of the results requires a sophisticated mathematical procedure based on curve fitting to various symmetrical peaks. Interpretation also involves comparing the modified sample to the reference spectra [62–64].

FTIR can also provide qualitative information about surface functionality. The analysis is based on the comparison of the wavelength of the peaks obtained to the spectra of known organic compounds [65]. Surface oxygen groups show their absorption bands at 3600, 1730, 1620, and 1260 cm^{-1} which represent OH, C=O, C – …O, and C–O stretching vibrations, respectively. Their relative intensities provide information about the possible arrangement of oxygen into various functional groups.

Information about the number of primary adsorption centers present in activated carbons can be obtained from an analysis of the enthalpy of carbon immersion in water. The relationship between these two quantities was proposed by Stoeckli et al. [27] as

$$\Delta H_i(\mathrm{J/g}) = -25.0(\mathrm{J/mmol\ H_2O})a_0 - 0.6(\mathrm{J/mmol\ H_2O})(a_s - a_0) \qquad (2)$$

where ΔH_i, a_0, and a_s are the enthalpy of immersion, number of primary adsorption centers, and limiting amount adsorbed, respectively. Using en-

thalpy of immersion one can analyze the changes in the degree of carbon oxidation, as has been shown by Rodriguez-Reinoso and coworkers [66,67].

None of the methods presented above are capable of providing completely reliable information about the quantity and quality of surface groups in carbons. Boehm titration is considered a very good method for evaluating the general trends in surface acidity. It is simple, fast, and usually gives reasonable reproducibility. Its major deficiency is that *all* groups with a pK_a in the range of the oxygen-containing species are classified as oxygen-containing acids. Therefore, the presence of other surface groups (containing for example nitrogen, phosphorus, or sulfur), whose pK_a is in this range, will lead to an overestimation of the number of oxygenated surface groups. Unlike the Boehm method, potentiometric titration allows the specific pK_a of various groups, in the categories defined by Boehm, to be obtained. Because many different heteroatom configurations can result in a similar pK_a (which also depends on the unknown activity of the solution), the exact classification of a species is impossible. TPD data can usually confirm the results of titrations; however, the number of detected groups is found to be larger by a factor of 2. The measurement is higher because titration methods are able to detect only acids and bases having a certain pK_a value, whereas during thermal desorption all surface groups, regardless of their chemical nature, should decompose. The TPD method can only be used to evaluate the surface chemistry of carbons that were obtained by carbonization at high temperature. In the case of low-temperature carbons (such as those obtained using phosphoric acid activation), the results are meaningful only at temperatures lower than those of the manufacturing process. The main weakness of the XPS method is the difficulty in identifying the type and distribution of functional groups unambiguously. In the case of FTIR, qualitative analysis of spectra is relatively easy. However, quantitative evaluation of the surface chemistry using FTIR is an extremely difficult task due to continued background absorption and the possibility of the presence of various functional groups as simple and non-associated structures.

3. Semi-empirical models

The most commonly used approach to describe and interpret water adsorption isotherms is that proposed by Dubinin and coworkers [4,5,67]. However, their models are not thermodynamically consistent at low relative-pressure [68] and the application of the approach has been successful for only certain carbon–water systems [4,18,20,25,27,37]. To understand the mechanism of the process they compared the dispersive interactions of benzene and water with graphite. A comparison of the reported values of benzene (14.3×10^{-51} J m^6 kmol^{-1}) and water (2.59×10^{-51}J m^6 kmol^{-1}) indicate that the dispersive energy for water adsorption on graphite is almost six times lower than benzene [4]. According to Dubinin and coworkers, this difference causes the enhancement of the adsorption potential of water in small micropores to be negligible, and therefore the mechanism of adsorption in microporous carbons should resemble that on a planar graphite surface. They assumed that the main cause for water adsorption is primary adsorption centers — surface oxygen groups. This assumption was based on the analysis of the differential heats of adsorption of water on activated carbons and graphites [29,30]. The values reported were nearly constant and equal to the latent heat of condensation for bulk water, suggesting that the interactions are equal in their nature to the interactions in bulk water (H-bonds). Because water–water interactions via H-bonds are much stronger than the water–carbon surface interactions (the energy of a H-bond is about 11 kJ mol^{-1} [31]), it follows that subsequent adsorption occurs on water molecules already adsorbed on primary adsorption centers [4]. The result is the creation of secondary adsorption centers. Based on this analysis, the dynamic adsorption condition can be described as:

$$k_2(a_0 + a)h = k_1 a \tag{3}$$

where a_0 is the number of primary adsorption centers, a the adsorption value for a relative pressure of $h = P/P_0$, and k_1, k_2 are kinetic constants. After rearrangement, the adsorption isotherm can be written as:

$$a = a_0 ch/(1 - ch) \quad (4)$$

where $c = k_2/k_1$. The parameters of the equation can be determined graphically from the linear form of the equation:

$$h/a = 1(a_0 c) - h/a_0 \quad (5)$$

Analysis of water isotherms obtained for carbon blacks and microporous carbons led to the conclusion that after adsorption on primary centers a monolayer of water is created with a thickness of about 0.55 nm. The formation of the monolayer is completed at $P/P_0 = 0.6$. This information can then be used for the calculation of the geometric surface area of the microporous carbons. According to Dubinin and coworkers, for carbons with larger micropores (e.g. 1.1 nm), after formation of the monolayer the pores are filled as a result of the weak dispersive interactions that cause an increase in the adsorption potential [4]. The water in the filled micropores can be considered as a condensed phase having a constant heat of evaporation. Consequently, the pores are emptied in a very narrow pressure range during desorption.

The approach described by Dubinin and coworkers, known as the Dubinin–Serpinsky method (DS), has often been used for the interpretation of adsorption data. The basic quantity derived using this approach is the number of primary adsorption centers, a_0, which can be easily determined by fitting the experimental data to the proposed isotherm [4,18,20,27,28]. This number is considered to represent the number of surface oxygen groups, such as carboxylic, lactonic, phenolic, and carbonyl [33].

For carbons with a low content of oxygen groups, experimental data have been fit successfully by the DS equation. However, for highly oxidized carbons the equation failed, especially in the low relative-pressure range. Evans [7] first mentioned the inapplicability of the DS equation to certain types of carbons in his study of adsorption in strongly oxidized carbons. He pointed out that the good fit to the DS equation in the low-pressure region was based on only a few points, and that the isotherm reported by Dubinin and coworkers started at a high value of relative pressure of $P/P_0 \sim 0.1$. When the isotherms were measured more precisely and the surface of the carbon was characterized by a high concentration of oxygen groups, the equation failed, suggesting a deficiency in the theory [7,19,20,33]. As a modification of the approach, Evans used the isotherms derived by D'Arcy and Watt [6], who proposed that three separate processes contribute to the sorption of water on heterogeneous sorbents. They are: (a) monolayer adsorption by strongly binding sites; (b) monolayer adsorption by weakly binding sites; and (c) formation of a multilayer — the extent of which is limited by the properties of the substrate. The equation has the following form:

$$a = \frac{KK'h}{1 + Kh} + Ch + \frac{kk''h}{1 - kh} \quad (6)$$

where K' and k'' are related to the number of primary and secondary sites, respectively, C is the Henry's law constant for adsorption on low energy sites, K is a function of the primary site–water interaction energy, and k is a function of the water–water interaction energy. The D'Arcy and Watt equation shows much better agreement with experiment at low relative-pressure than the DS equation [7] for the isotherms measured by Evans [4], as seen in Fig. 10. However, the equation gave poor results at high pressure for this system.

Analysis of the validity of the parameters of the DS equation by Barton et al. [34] showed that the equations proposed by Dubinin and coworkers only work well for certain groups of carbons. The authors found good agreement of the parameters obtained with independently measured surface oxide concentrations and enthalpy of immersion. Following the DS approach, they formulated the cubic form of equation (DS-3) which should apply only if $a_0 \ll a$. It has the following form:

$$-cka^3 - cka_0a^2 + ca = a/h \quad (7)$$

Analysis of the fitting of the three forms of the DS equation to various carbons along with the values obtained for a_0, led to the conclusion that two oxygen atoms are required to form a primary site since there is no one-to-one correspondence between these quantities [34]. It was proposed that the mean enthalpy of interaction (calorimetric enthalpy, ΔH_i, divided by the total amount ad-

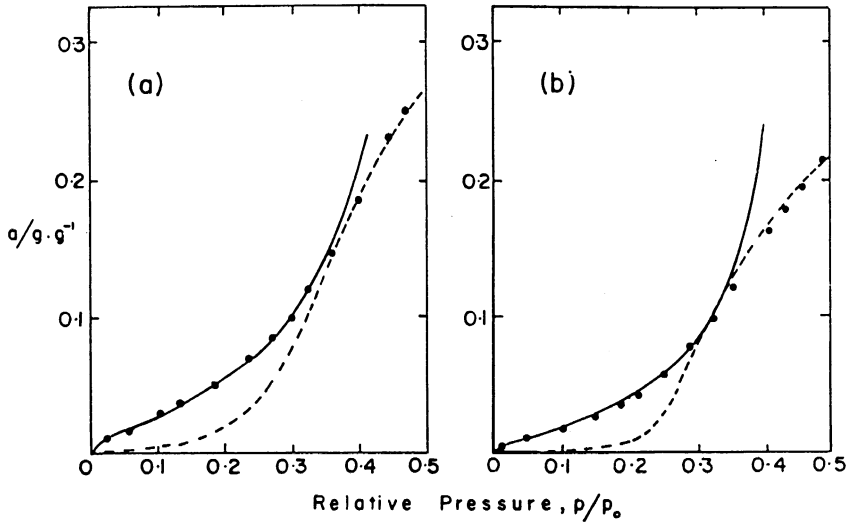

Fig. 10. Comparison between experimental (points) and fitted isotherms: broken line, DS-equation; solid line, D'Arcy and Watt equation — (a) 2 h oxidation, (b) 7 h oxidation [7]. Reprinted from Ref. [7] with permission from Elsevier Science.

sorbed taken from isotherm analysis) should increase with increasing number of primary adsorption sites if the primary interaction is much more exothermic than the H-bonding interactions. Analysis of the relationships obtained suggested that the 1.3 kJ mol^{-1} intercept represents the enthalpy of the H-bonding interactions on an unoxidized carbon surface.

Based on an analysis of water adsorption isotherms and enthalpy of immersion, Stoeckli et al. [11] proposed that isotherms of Type IV (frequently observed for water adsorption) can be expressed using the Dubinin–Astakhov (DA) [69] equation as a superposition of Type I and Type V isotherms. They found that the molar heats of immersion for the initial part of the isotherms should be in the range of 5–8 kJ mol^{-1}, which represents the interaction of water with acidic centers. The second part of the isotherm corresponds to adsorption by hydrophilic centers, which are probably of the carbonyl type. The approach based on the DA equation was applied in an extensive study of water adsorption on oxidized carbons by Carrasco-Marin and coworkers [32]. The adsorption energies for Type I and Type V isotherms were comparable to those obtained previously by Stoeckli et al. [11]. Their calculation based on multiple linear regression showed that for the first isotherm region there are ca. 3 water molecules interacting with the carboxylic and lactonic groups, and ca. 1.5 molecules interacting with the phenolic and basic groups. The energy balance led to the interactions of carboxylic, lactonic, phenolic, and basic groups to be 17.4, 17.5, 9.5, and 10 kJ eq^{-1}, respectively. It follows that specific contributions of water molecules attached to the group are similar (6.2–6.8 kJ mol^{-1}).

The approach based on the Dubinin–Astakhov equation was also proposed by Lodewyckx and Vansant [16]. They showed that the parameters obtained from nitrogen adsorption isotherms such as the micropore volume, W_0, and characteristic energy of adsorption, E_0, can be used to fit water isotherms to the DA equation using the affinity coefficient, $\beta = 0.063$. The authors were aware that in the first region of the isotherms, especially for oxidized carbon, a satisfactory fit cannot be obtained using the proposed approach. Nevertheless, in the second region of the isotherms (where micropore filling occurs due to water–water interactions) an excellent fit was reported [16]. The method, although inapplicable for carbons having oxygen groups, satisfactorily predicts the capillary condensation region of the isotherm (see Fig. 11).

Another isotherm describing water adsorption was proposed by Talu and Meunier [8]. Their isothermal data are represented by three parameters: Henry's constant, saturation capacity, and reaction constant for cluster formation in micropores. The Talu and Meunier expression is:

$$P = H\Psi/(1 + K\Psi)\exp[\Psi/(N_m)] \quad (8)$$

where H is Henry's constant, K the association constant, Ψ the surface coverage at the pressure P, and N_m is the saturation capacity. The theory used to derive the isotherm equation assumes that at low pressure the behavior of the system is controlled by vertical interactions of a molecule to the surface and that the molecules are adsorbed on active sites. At intermediate coverage where the inflection point occurs, the adsorbed molecules form clusters via H-bonding. At high surface coverage where a plateau is noticed, the adsorption is limited by the micropore volume. To test the theory, the authors used type V isotherms and a good fit was obtained. However, in the cases where some uptake existed at low relative-pressure, the theory significantly underestimated the amount adsorbed (see Fig. 12).

Recently Do and Do have proposed a new model to describe the adsorption equilibrium of water in activated carbons [68]. It is based on the growth of a water cluster around the surface functional groups, the creation of a pentamer, and its adsorption in micropores. The equation derived by Do and Do has the following form:

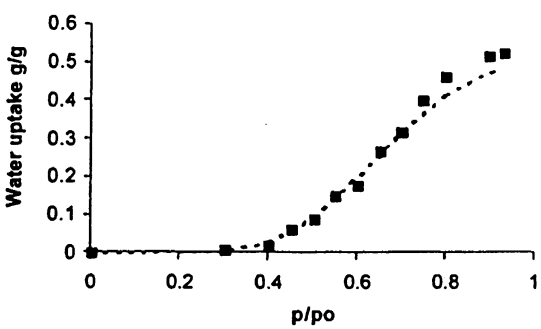

Fig. 11. Fitting (- - -) of the experimental water isotherm (squares) on R1Extra carbon with DA equation [16]. Reprinted from Ref. [16] with permission from Elsevier Science.

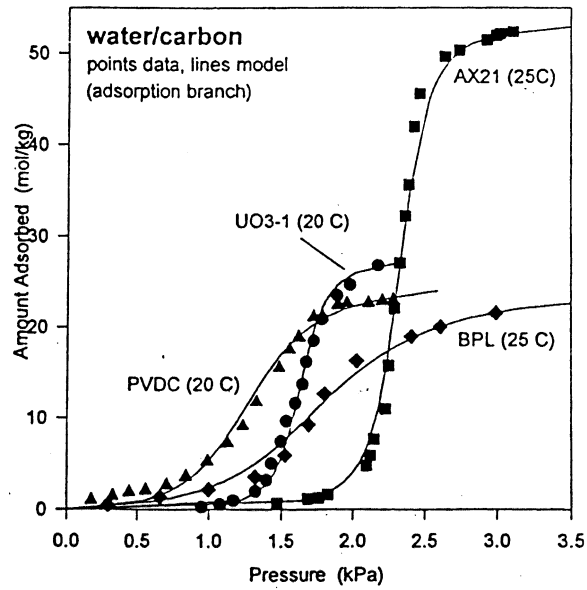

Fig. 12. Comparison of experimental data (points) with the correlation of Talu and Meunier (lines) for water adsorption on several carbons. Taken from Ref. [8]. Reproduced with permission of the American Institute of Chemical Engineers. Copyright © 1996 AIChE. All rights reserved.

$$C_\mu = C_{\mu S}\frac{K_\mu \sum_{n=6} x^n}{K_\mu \sum_{n=6} x^n + K_\mu \sum_{n=6} x^{n-5}} + S_0\frac{K_f \sum_{n=1} x^n}{1 + K_f \sum_{n=1} x^n} \quad (9)$$

where C_μ, x, S_0, K_f, K_μ, and $C_{\mu S}$ are the total water adsorbed concentration, reduced pressure of water, functional group concentration, chemisorption equilibrium constant, micropore equilibrium constant, and saturation concentration in the micropore, respectively. The authors propose that S_0 can be found from a chemisorption titration experiment, the saturation concentration in the micropore from the adsorption data in the neighborhood of $x = 1$, and the two equilibrium constants can be found from an optimization between the theory and the experimental data. The isotherms obtained, with some parameters fitted to the experimental data, showed good agreement.

4. Molecular models and simulation methods

The validity and reliability of any molecular simulation study hinges on the realism of the models used for the porous carbon and for the interaction potentials. While a detailed model that accurately represents the system of interest is desirable, it must be simple enough that the calculations remain tractable. This has been an important criterion in developing water potentials and also models of the carbon structures. Below we examine the current state of the available models for the porous carbon, the intermolecular potentials of water, and for the various chemical groups present on the carbon surface. We also review molecular simulation methods commonly used to study adsorption in porous media.

4.1. Models for porous carbons

In order to characterize activated carbons in a manner that is reasonable for molecular simulation work, we must simplify our model of the pore structure. The most common means of doing so, involving an idealized representation of the pores, is the slit pore model. In this model one assumes that guest molecules adsorb in pores that are planar and slit-like in geometry, wherein a pore is represented as the space between two graphite-like crystallites. The model is generally constructed such that these crystallites are semi-infinite and composed of perfect graphene sheets layered and aligned parallel to one another (see Fig. 13). The crystallites are further assumed to be structurally equivalent to graphite, with the corresponding density and interplanar separation. The pertinent model dimension is the pore width H, defined as the distance between the two parallel faces of the crystallites. In practice it is usual to regard a given carbon as made up of slit pores having a distribution of pore widths, this distribution corresponding to some rough estimate of the pore size distribution for the carbon of interest.

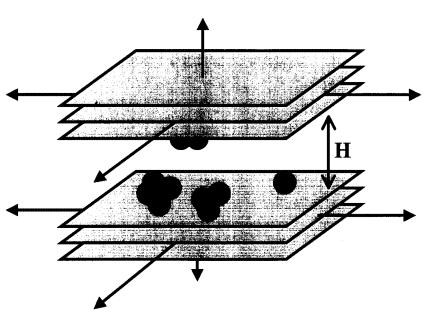

Fig. 13. The slit pore model of porous carbons.

The basis of the slit pore model is empirical — justified by experimental observations of real activated carbons. A typical TEM micrograph of an activated carbon shows roughly this sort of pore environment. Pore regions can often be identified that locally resemble slit-like pores. However, depending on the size and deformation of the graphite-like crystallites, the 'slit-like' geometry is often rough at best, and highly dependent on the material studied. The advantage of the slit pore model is that it is purely geometric. Thus one can study confined fluid behavior and adsorption within a whole class of materials without being confined to a specific carbon structure.

The slit pore model has been used extensively to study adsorption in porous carbons (e.g. Refs. [70–76]). Despite its success, the model's assumptions bring into question the applicability of the model to highly activated carbons. First, adsorption is restricted to flat (often smooth) crystallite surfaces. Second, the crystallites are typically assumed to extend to infinity (through the use of periodic boundary conditions). These two assumptions preclude the possibility of adsorption along the edges of crystallites. Third, the pore regions in real activated carbons have complicated topologies and connectivity — a feature that is non-existent in the slit pore model. The true pore topology of an activated carbon provides long-range correlation effects that may be significant to the thermodynamics of adsorbed fluids, particularly near the critical point regions of fluid–fluid phase envelopes.

There have been several models proposed to account for the deficiencies in the slit pore model. Recently McEnaney et al. [77] proposed a model allowing for a variable number of carbon plates per crystallite. In this manner, one can account for differences in the local carbon density as well as adjust the thickness of the bounding crystal-

lites. Also, by varying the inter-graphene plate separation, the model is much more flexible and can (to some extent) be 'tuned' to incorporate experimental characterization data. Rodriguez et al. [78] proposed a model constructed from carbon sheets of finite size arranged in parallel (yet offset) arrangements and linked to one another through oxygen bridges. Although limited in its spatial extent, the model does offer a pore topology that is qualitatively more accurate. Another model that deviates from the slit pore model was suggested by Segarra and Glandt [79] and is based on the work of Eppenga and Frenkel [80]. In their model, a random distribution of graphene platelets is generated in a periodic simulation cell. Similarly, Dahn et al. [81] suggested the *falling cards model*, in which graphene plates are arranged through a procedure that mimics cards falling on top of each other. These types of models have the advantage of retaining the carbon geometry of layered graphene crystallites, yet incorporating long-range pore topologies.

Seaton et al. [82] recently proposed a modification of the slit pore model called the 'randomly etched graphite' (REG) model. In this model one conceptually begins with a slit pore. From there, carbon atoms are randomly removed from the surface graphite planes of the pore, producing a pore geometry that is slit-like, yet rough on the surfaces. This roughness addresses the assumption of smooth pore walls in the slit pore model, and allows for structural heterogeneity in the graphene plates themselves. In real activated carbons, crystallites often contain defects in the form of non-aromatic carbon rings. These defects produce non-planar surfaces that can be qualitatively approximated by this model. Other models have been proposed to account for surface heterogeneity. For instance, Bojan and Steele [83] suggested a model in which truncated graphite basal planes are stacked to produce a stepped surface.

In an attempt to preserve the structural aspects of real activated carbons, and at the same time to provide a realistic pore representation, Thomson and Gubbins [84] have recently suggested a model based on reverse Monte Carlo (RMC) [85–87]. The RMC model takes, as input, the experimental carbon–carbon radial distribution function obtained from SAXS and X-ray diffraction data (XRD). One starts from a system composed of single-layer graphene crystallites having a range of sizes, placed randomly in a box; the size distribution is described by a Gaussian distribution about a mean size (typically 1–5 nm) that is believed to represent that of the real carbon of interest. Through a series of Monte Carlo moves, the simulated radial distribution function (RDF) is successively refined to match experiment. The procedure is limited by the constraints made on the carbon structure. In this case, the assumption of perfect graphene plates of carbon is used — although the size and shapes of the plates are allowed to change. By adding and deleting aromatic rings from the graphene plates, and by randomly perturbing their positions and orientations, a method is generated whereby the carbon model propagates into a configurational minima with respect to the experimental RDF. The model is powerful in that it generates a representation of the activated carbon that contains a pore topology closely approximating the true topology of the real carbon (see Fig. 14). Furthermore, the representation can be used in large-scale simulations of adsorption and confined fluid phenomena. The RMC method is amenable to further refinement. For example, it is possible to allow defects and curvature of the graphene crystallites through trial replacement of aromatic rings with defective ones. A problem with the use of SAXS and XRD data as input is that they do not appear to be sensitive to the larger mesopores. Thus this approach is best suited to the determination of the micropore structure. It is possible that the use of TEM or other structural data as input may be more sensitive to the larger pores.

The RMC model's main advantage is the incorporation of experimental radial distribution functions directly into the calculation, but a prudent choice of the target density is essential. The RMC model will generate the best-fit structure for a given target density. However, a relatively broad range of densities could be specified, resulting in different output structures for a given radial distribution function. The local carbon density is an input to the model and cannot be realistically predicted from the radial distribution function.

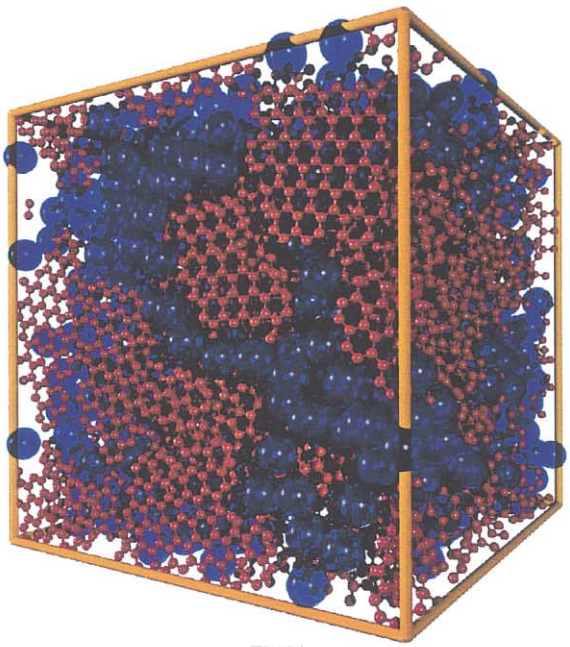

Fig. 14

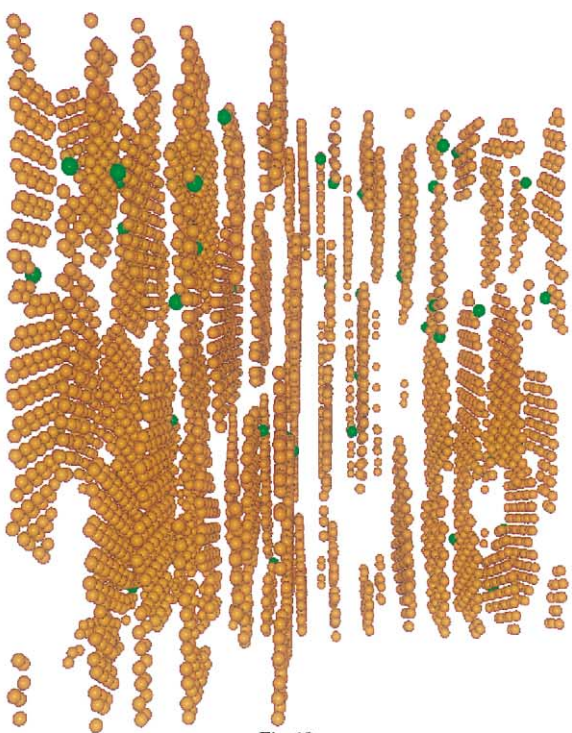

Fig. 18

Therefore, accurate density measurements are required to give a meaningful predicted structure. The RMC model should also be used with caution for carbons of non-uniform density. The RMC method applied to such carbons — exhibiting large fluctuations in local density on a length scale larger than the simulation cell of the model — cannot give a reasonable representation of the entire pore structure.

Once a suitable model is generated, simulation work can proceed using whatever type of interaction potentials are desired. The main importance of the structural carbon model is to provide a realistic representation of the pore environment. Despite these recent advances in carbon modeling techniques, the majority of simulation of work on water in carbons so far has been based on the slit pore model. Nevertheless, the slit pore model is useful in that it provides a phenomenological description of water adsorption in carbons. Such work is important in that it provides the groundwork for characterizing water adsorption in more realistic carbon structures, where the shape and connectivity of the pore regions are expected to play critical roles in accurately describing these phenomena.

4.2. Intermolecular potentials for water

Despite many attempts, an intermolecular potential model for water that is valid over a broad range of state conditions and produces satisfactory results for a variety of properties remains elusive [88–91]. As in any such model development, optimization of the intermolecular parameters are determined by either fitting potential parameters to experimental data or from ab initio

Fig. 14. A model of a microporous activated carbon prepared by the RMC procedure [84]. Small spheres connected by bonds are the carbon atoms (drawn to reduced scale to make the structure clearer). Large spheres are adsorbed nitrogen molecules.

Fig. 18. A carbon model prepared by the RMC method, to which surface sites (green spheres) have been added at random points on the edges of the graphene microcrystals. For visual clarity, the size of all spheres has been reduced and one-quarter of the simulation box at the right front edge has been removed.

quantum mechanical calculations. For current water models, ab initio calculations cannot capture dispersion and many-body effects with accuracy comparable to that of empirical effective potentials (although a recently proposed fluctuating-charge model fit to ab initio data successfully reproduced the liquid structure at ambient conditions [92]). Therefore, typically the intermolecular potential parameters of proposed water models are optimized to reproduce a given set of experimentally measured properties. Most of these empirically derived potentials can be divided into two categories: (a) fixed point-charge models; and (b) models that account for polarizability, i.e. the phenomenon of a fluctuating charge responding to a changing local electric field.

Fixed point-charge models have simple molecular force fields described by arrangements of charges located in well-defined geometries. Most often a Lennard-Jones potential is used to account for van der Waals (non-polar) type forces, while fixed charges [93–99] or square-well sites [100–103] describe the electrostatic (polar) interactions. An obvious defect in fixed-charge models is that the electrostatics cannot respond to a varying local electric field and consequently are unable to describe the considerable polarization effects that can occur, for example, in condensed phases. Additionally, non-polarizable water potentials suffer from a lack of transferability in that they are unable to describe both the two-body interactions of an isolated molecular pair and the many-body interactions of the condensed phase without encountering undesirable state-dependent parameters [91].

Augmentations of fixed point-charge models have followed several routes. Additional interaction sites have been introduced to represent a charge distribution [104], non-pairwise additive effects accounted for via charge or dipole polarizabilities [105–112], flexible geometry models have been proposed [113–115], as well as models combining both flexible geometries and polarizibility [116–118]. These more detailed models frequently require a substantial increase in computational expense and so far have not exhibited an obvious improvement in the description of both the thermodynamic and structural properties. Additionally, the increased computational requirements of polarizable models do not permit extensive systematic parameterization studies. Achieving a balance of accuracy, transferability, and tractable computations has led to the popularity of fixed point-charge models.

The merit of a potential model is typically judged by how well the model describes the thermodynamics of the system (particularly vapor–liquid equilibria) and the liquid structure (as measured by the radial distribution functions $g_{HH}(r)$, $g_{OH}(r)$, and $g_{OO}(r)$). It is important that the model can describe these properties over a significant range of densities, particularly when simulating water in porous carbons, since the bulk and confined phases can be at considerably different densities for a given temperature. A recently proposed fixed point-charge model by Errington and Panagiotopoulos [89] has been successfully optimized to reproduce the vapor–liquid equilibria over the entire temperature range from sub-ambient to the critical point. As illustrated in Fig. 15, it is superior to other fixed point-charge models in its description of the vapor–liquid phase envelope. It also more accurately predicts the vapor pressure, the second virial coeffi-

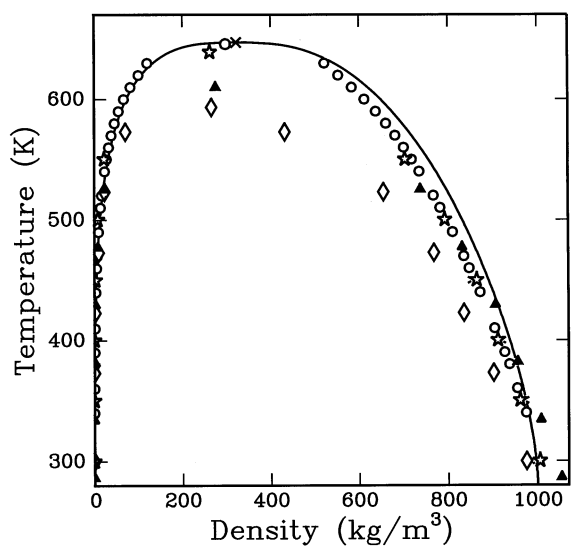

Fig. 15. Vapor–liquid equilibria for water. Diamonds, stars, triangles, and circles represent calculations for the SPC [97], SPC/E [98], MSPC/E [99], and Errington and Panagiotopoulos [89] models, respectively. The line shows the experimental results. Reprinted with permission from Ref. [89] copyright 1998, American Society.

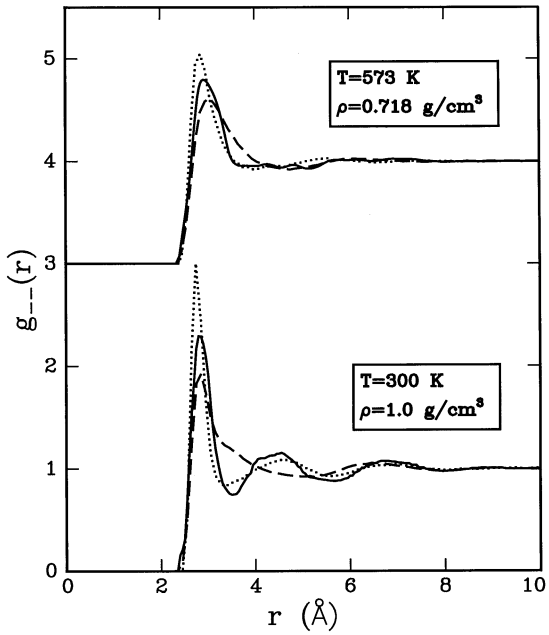

Fig. 16. Negative–negative (oxygen–oxygen) pair correlation functions for water. Dashed, dotted, and solid lines are used to represent the Errington and Panagiotopoulos [89] model, the SPC/E model [98], and experimental data [191], respectively. Reprinted with permission from Ref. [89] copyright 1998, American Chemical Society.

cient, and the critical parameters. In particular, it outperforms the widely used SPC/E [98] model in its description of $g_{HH}(r)$ and $g_{OH}(r)$, and is similar for $g_{OO}(r)$. However, besides the previously mentioned drawbacks of any fixed point-charge model, the model fails to describe the second peak in $g_{OO}(r)$ (see Fig. 16) and predicts a dielectric constant that is too low by about 25% at 300 K. Additionally, the Errington and Panagiotopoulos model [89] encounters an unusual difficulty when determining unlike-pair interaction parameters. The model accounts for non-polar pair interactions with a Buckingham Exp-6 potential (three-parameter potential). However, the majority of parameterized potentials (e.g. optimized potentials for liquid simulations (OPLS)) use a Lennard-Jones potential to account for the non-polar interactions (2-parameter potential). Therefore, determining unlike-pair interactions may prove troublesome — although a recent publication suggests a direct solution [119].

The most serious defect in the simulation of water in porous carbon using any fixed point-charge model may be the crude treatment of polarizability effects. Although the inclusion of many-body polarization does not appear to offer a significant improvement in the description of the thermodynamics and structure for bulk water [88,90,120,121], it may prove vital for water near a carbon surface. Such effects are likely to be of particular importance for confined aqueous mixtures since selective adsorption will be affected by dissimilar polarizibilities of the mixture components induced by the carbon surface. Of the available models that include many-body polarization, those proposed by Errington and Panagiotopoulos [122] and by Chialvo and Cummings [123,124] are of particular interest, since again, the potentials are optimized using wide-ranging thermodynamic and structural data.

4.3. Water–substrate interactions

Water–substrate interactions are of two kinds, those with the carbon surfaces and those with oxygenated surface groups. It is common to assume that water–carbon interactions include only dispersive and repulsive contributions, and they are commonly modeled using the Steele 10-4-3 potential [125] given as

$$u_{cf}(z) = 2\pi\rho_c\varepsilon_{cf}\sigma_{cf}^2\Delta\left[\frac{2}{5}\left(\frac{\sigma_{cf}}{z}\right)^{10} - \left(\frac{\sigma_{cf}}{z}\right)^4 - \left(\frac{\sigma_{cf}^4}{3\Delta(z+0.61\Delta)^3}\right)\right] \quad (10)$$

where the density of the carbon is $\rho_c = 114\ \text{nm}^{-3}$, the separation of the graphite planes is $\Delta = 0.335$ nm, and ε_{cf} and σ_{cf} are the Lennard-Jones parameters for the interaction between carbon atoms and water. The carbon–carbon potential parameters are taken as $\varepsilon_{cc}/k = 28$ K and $\sigma_{cc} = 0.340$ nm [125]. Interaction parameters can be adjusted to fit extremely low-pressure adsorption data (for which the fluid–fluid interactions are negligible).

Surface oxygenated groups are typically modeled with standard potentials such as OPLS functions [126] or DREIDING force-field potentials [127]. These potential models consist of Lennard-Jones

potentials plus fixed point-charges intended to mimic H-bonding. Other studies have replaced the point charges with off-center square-well potentials [14,128]. This approach lessens some of the computational burden since the square-well potential is short ranged. Additionally, the highly localized attractive character of the potential may more realistically model H-bonding. Interesting attempts have been made at mimicking the activation by incorporating surface functional groups as dipoles, evenly smeared around the edges of graphitic carbon platelet disks [79]. However, recent work suggests the model is not sufficiently inhomogeneous to predict the correct trends in low-pressure adsorption and in the heats of adsorption [129].

In Section 2.2, we saw that a variety of functional groups (e.g. phenolic, lactonic, carboxylic, hydroxyl, carbonyl) can be present on the surface (see Fig. 9). Experimental characterization of the surface chemistry can be achieved using a variety of chemical and physical techniques. Frequently, different methods lead to quite disparate results, presumably due to the complexity of the carbon structure. Recent experiments [130] and simulation studies [131] suggest that, on average, the interaction appears to be roughly independent of the type of active surface group in which the oxygen is incorporated. Therefore, mixtures of surface groups have been represented as an effective single group from a suitably weighted mean of the total site–water interactions [14]. Although idealized, the use of an effective site model is a logical choice and can simplify the analysis of the adsorption mechanism. Examples of surface site models for a single slit-like pore model and for a more realistic model (as discussed in Section 4.2) are shown in Figs. 17 and 18, respectively.

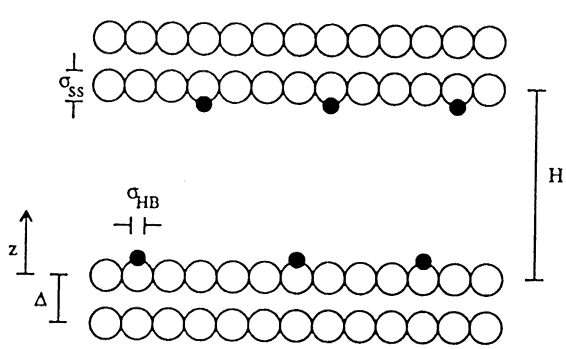

Fig. 17. A slit pore model in which the carbon surfaces are decorated with surface sites (black spheres). Reprinted with permission from Ref. [13] copyright 1996, American Chemical Society.

These simple models often capture the predominant behavior of water adsorption; however, they omit some interactions that may be significant and could limit their predictive capabilities. Among the most important interactions that are neglected are: (1) direct electrostatic interactions between water molecules and the carbon surface; (2) induction interactions between water molecules and the carbon surface; (3) induction interactions between water molecules and the oxygenated surface groups; and (4) higher order two-body dispersion and three-body interactions. For the direct electrostatic interactions between the fluid molecules and the carbon surface electric field, recent studies suggest the use of surface quadrupoles located in the carbon basal plane [132–136]. The influence of induction effects, due to interaction between charges on the water molecules with the induced dipole in the graphite and oxygenated groups, can be estimated via the usual many-body induction terms [137]. In these calculations, it is important to include the effects of anisotropy in the polarizability of graphite [138,139]. Higher order two-body dispersion and three-body fluid-substrate interactions have been considered by several authors [131,139–143]. For simple non-polar fluids interacting with graphite, these forces are believed to contribute 5–15% of the total fluid–substrate energy [139–142].

Having chosen reasonable potential models for the surface groups, the sites need to be placed in the carbon structure. X-ray diffraction studies show that these groups are randomly located around the edges of the carbon microcrystallites [144]. The relative and absolute amounts of the groups depend on the carbon precursors and the activating process. Experimental site densities range from 0 to 2.65 sites nm^{-2}. The density and placement of the surface sites can be guided by experimental characterization data.

4.4. Molecular simulation methods

The principal method that has been used to study adsorption in confined systems is the grand canonical Monte Carlo (GCMC) simulation method. The technique mimics adsorption experiments by simulating an adsorbed fluid in equilibrium with a bulk fluid reservoir. The GCMC method simulates an open system specified by fixed temperature T, volume V, and chemical potential μ. Any Monte Carlo simulation method uses a Markov chain to generate a series of molecular configurations with the correct distribution of energy and density. In the grand canonical ensemble, the probability associated with any given state s of the system is

$$P(s) \propto \exp[-\beta(U(s) - N\mu) - \ln N! - 3N \ln \Lambda + N \ln V] \quad (11)$$

where Λ is the deBroglie wavelength, $\beta = 1/k_b T$, $U(s)$ the total intermolecular potential energy of the system, and N the number of molecules in the system. The most common prescription for generating the Markov chain [145,146] modifies the current molecular configuration in one of three ways: (i) creation of a new molecule at a random position; (ii) deletion of an existing molecule; or (iii) displacing an existing molecule by a random vector. The new configuration is accepted or rejected according to criteria (founded on rigorous statistical mechanics) that involve the temperature and the chemical potential. Thermodynamic quantities of interest (e.g. internal energy or density) can be estimated by averaging instantaneous values over a large number of configurations. Statistical efficiency and simulation lengths vary widely between different systems. For example, the probability of accepting an attempted molecule creation can be extremely low for high-density systems or systems in which the intermolecular potential depends strongly on the relative molecular orientation. This latter condition is especially pertinent to the simulation of water since strong H-bonds are likely to form. Not only is it necessary to find a position that does not overlap with another water molecule, but it must also have an acceptable orientation. Because the number of trial creations can be prohibitively high when simulating water, biased sampling techniques must be employed (see, e.g. Ref. [147]).

Experimental adsorption isotherms are generally reported as the amount adsorbed as a function of the pressure of the bulk fluid, P/P_0, where P_0 is the bulk fluid saturation pressure. Since in a GCMC simulation the chemical potential rather than the pressure is specified, a suitable equation of state (EOS) is used to relate the chemical potential to the pressure. A recent novel simulation method facilitates this process for adsorption studies of fluids for which a suitable EOS is not known a priori [148].

An important refinement in the use of GCMC simulations to study capillary phase equilibria was the development of an integration scheme that precisely locates the thermodynamic condensation pressure in mesoporous systems [149]. The method has been used to study liquid–vapor coexistence in both cylindrical models [150] and more complex models [151,152]. To date, explicit determination of phase transitions have not been performed for water in activated carbons, but a number of simulation techniques are available for future work. A well-established bulk fluid simulation technique, the Gibbs ensemble Monte Carlo (GEMC) method [153,154], directly calculates phase coexistence by simultaneously simulating the coexisting phases in two different simulation cells. Both mass and volume is exchanged between the two phases, with acceptance criteria which impose equality of pressure, temperature, and chemical potential between the phases. For confined systems of idealized pore geometries (single slit pores and cylinders), the method has been used to determine capillary condensation [155,156] and liquid–liquid phase diagrams [157]. For more realistic pore models, Gordon and Glandt [158] used GEMC to simulate a symmetric binary liquid–liquid mixture, while a recent extension of the method allowed a systematic study of the vapor–liquid phase behavior of pure fluids [159] and fluid mixtures [160] in random porous media.

Yet another simulation technique for studying confined fluids is the semi-grand Monte Carlo method developed for determining multi-component phase equilibria [161]. For a binary mixture, it consists of a simulation at constant (T, N, $\mu_1 - \mu_2$), which is achieved by including simulation moves that attempt to interchange the species of the

molecules. The absolute chemical potential of both species can be calculated using a modification of the Widom insertion method [161]. The semi-grand method can be used for studying liquid–liquid coexistence in pore systems [162,163]. It has the advantage over GCMC that the molecule insertion and deletion steps are replaced by species exchange steps, which are more easily carried out at high density.

Another class of methods, termed *histogram analysis* [164–168], allows the bulk phase coexistence and critical point data to be obtained with high precision. The methods are based on the collection and analysis of histograms of the energy and number of particles during a Monte Carlo simulation. The density of states and free energies in the system can be extracted from these histograms. In the grand canonical ensemble, the probability of observing a state s with given $\Omega = U(s)$ and N is given by Eq. (11). Equivalently, the probability of observing a state with energy Ω and number of particles N could be written as

$$P(\Omega,N) \propto \exp(\beta\mu N)\exp(-\beta\Omega) \times W(\Omega,N) \quad (12)$$

where $W(\Omega,N)$ is the microcanonical density of states of energy Ω and number N. In a given GCMC simulation, histograms of the energy and number of particles are collected. The height of each histogram will be proportional to $P(\Omega,N)$, so that the density of states can be recovered (up to a constant factor) from the simulation data by dividing by the Boltzmann factor and the chemical potential term. The probability $P(\Omega,N)$ can be estimated from different temperatures and chemical potentials (indicated with $'$), by reweighting the histogram according to

$$\frac{P_{\beta',\mu'}(\Omega,N)}{P_{\beta,\mu}(\Omega,N)} \propto \exp((\beta'\mu' - \beta\mu)N) \times \exp(-(\beta' - \beta)U) \quad (13)$$

The new distribution can be used to regenerate quantities such as $\langle\Omega\rangle$ and $\langle N\rangle$ and to locate thermodynamic transitions. A closely related technique is the histogram-biased Monte Carlo simulation method that biases the Monte Carlo chain to favor particular areas of phase space [169–171]. The resulting biased probability distribution histogram can then be corrected after completion of the simulation. From a single series of simulations, the technique allows the computation of the free energy barrier between two states (e.g. conformations or phase transitions) or the computation of the free energy of a system that cannot be equilibrated by conventional means because of extremely high free-energy barriers.

Recent applications of the histogram analysis method based on an order parameter formulation have been used to study solid–fluid transitions in pores [172]. The GCMC method is used to calculate the Landau free energy [173] as a function of an effective bond orientational order parameter, Φ. The Landau free energy is defined by

$$\Lambda(\Phi) = -k_b T \ln(P(\Phi)) + \text{constant} \quad (14)$$

where $P(\Phi)$ is the probability of observing the system having an order parameter value between Φ and $\Phi + \delta\Phi$. The probability distribution function $P(\Phi)$ is calculated as described above. The grand free energy Ω is then related to the Landau free energy by

$$\exp(-\beta\Omega) = \int d\Phi \exp(-\beta\Lambda(\Phi)) \quad (15)$$

where the integration is over the permitted range of Φ. In the work of Radhakrishnan and Gubbins [172], suitable order parameters were developed for studying freezing in slits (activated carbon fibers) and cylinders (silicas) as well as to study hexatic phases.

Monte Carlo simulation methods are restricted to the calculations of equilibrium quantities. Often we are interested in studying the dynamic behavior of a system, e.g. the diffusion of alkanes through activated carbons. Molecular dynamics (MD) simulation is a technique to compute the transport properties of a system. MD is a widely used method in which the classical equations of motion for a system are integrated using a finite-difference algorithm. The resulting trajectory samples the microcanonical ensemble of states, and can be used to obtain thermodynamic averages and transport properties. Most MD studies of phase equilibria in confined systems have focused on the kinetics of the two-phase separation. In these studies a system is quenched from supercrit-

ical conditions into the two-phase region. This method has principally been used to study liquid mixture separations in slit-pores [174], two-dimensional 'strip' pores [175], cylindrical pores [162,176,177], and more complex disordered media [178].

For a more comprehensive treatment of these methods the reader is referred to the texts: Computer Simulation of Liquids [146]; Understanding Molecular Simulation [147]; and Computer Simulation and the Statistical Mechanics of Adsorption [179].

5. Molecular simulation studies

There has been little simulation work on the adsorption of water in activated carbons. All studies have used the idealized slit pore model described in Section 4.1, with one exception [79]. Segarra and Glandt [79] used the SPC point-charge water potential and modeled the activated carbon using randomly orientated platelets of graphite with a dipole distributed uniformly over the edge of the platelets to mimic the activation. Recent work suggests the model of the surface sites is not sufficiently inhomogeneous to predict the correct trends in low adsorption data and in heats of adsorption [129]. Below we describe the simulation studies of the behavior of water in both graphitic and activated carbons modeled as slit pores. We also describe simulation work underway in more realistic carbon model structures.

5.1. Slit pore models

For graphitic carbons (where all the oxygenated groups have been removed from the surface through heat treatment or reduction) the adsorption behavior of water is dominated by the water–water interactions since they are much more attractive than the water–carbon interaction. Modeling graphitic systems is relatively straightforward and has been successfully carried out using both point-charge and off-center square well models of water in slit graphitic pores [13,14,180–183]. The adsorption behavior is characterized by negligible adsorption at low-to-moderate relative-pressures (see Fig. 19) followed by an onset of pore filling that occurs suddenly at high relative-pressures, $P/P_0 \sim 0.8$ for the model shown [13]. The adsorption behavior is Type V in the IUPAC classification and agrees satisfactorily with experiment [3,184]. Not surprisingly, such Type V behavior can be described with simple Lennard-Jones potentials [44] since the behavior merely requires a fluid–fluid interaction that is much more attractive than the fluid–solid interaction.

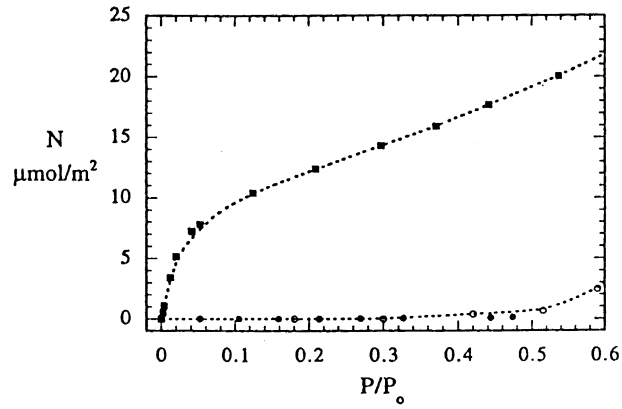

Fig. 19. Simulated adsorption isotherms for water (closed circles) and propane (squares) on a graphite surface at 300 K [13]. Open circles are experimental results of water on graphon at 20°C [192]. Dashed lines are drawn as a guide to the eye. Reprinted with permission from Ref. [13] copyright 1996, American Chemical Society.

Molecular simulation studies of activated carbons in which a significant density of oxygenated sites are present on the carbon surfaces are considerably more difficult to model. Maddox et al. [183], Muller and coworkers [13,185], and McCallum et al. [14] have used models in which the pores are approximated by slits comprised of graphitic walls, with embedded surface sites. In the work of Maddox et al. [183], the sites were assumed to consist of –COOH groups and were modeled using OPLS functions [186], while water was modeled using the TIP4P potential [96]. The adsorption isotherms of water at 298 K in a 2 nm pore with various site densities were obtained. More detailed studies have been carried out by Muller et al. [13] and McCallum et al. [14] for a wide range of surface site densities at 300 K. In these works, H-bonding between water molecules

and between water and a surface site was modeled using off-center square well potentials instead of charges. Interestingly, both the point-charge and square well models used to represent the H-bonding in these studies gave qualitatively similar results.

The objective of these studies was to examine the effect of active surface sites (e.g. OH, COOH, CO) on the adsorption of water. The size of graphite microcrystals, site density, pore size distribution, and site species were taken into account [14,187,188]. The adsorption behavior was found to depend strongly on the geometric arrangement of the active sites on the carbon surface. Results were obtained for both regular arrays of surface sites, and for randomly placed sites. Cooperative adsorption effects were found to be very important, with water clusters forming readily in surface regions where two or more sites were positioned at a separation suitable for both water–site and water–water bonding. The adsorption behavior was also found to be dependent on the number of sites present on the surface. When even low density of active sites are added to the carbon surface, the adsorption behavior is qualitatively changed. Adsorption of water is appreciable at low pressures, and pore filling occurs at lower pressures. At low pressures, isolated water molecules bond to oxygenated surface sites, but this stage is quickly followed by the buildup of water clusters around those sites. Where possible, water molecules seek locations where they can form multiple H-bonds on adsorption, either by bonding to several pre-adsorbed water molecules or to a water molecule and a surface site. At site densities of $n \sim 0.4$ sites nm^{-2} and above, capillary condensation no longer occurs but is replaced by a continuous filling of the pore. The effect of surface site density on the adsorption of water in a pore width of 1.69 nm is shown in Fig. 20. For experimental activated carbons, site densities usually range between $n = 0.1$ and 2.5 sites nm^{-2} (for comparison, there are about 38 carbon atoms nm^{-2} on a graphite surface). A comparison of simulation results with experimental data for a carbon having a site density of 0.675 sites nm^{-2} is shown in Fig. 21.

Generally good agreement is obtained with the model of McCallum et al. [14], despite uncertainties in the morphology of the carbon, which had a wide pore size distribution. However, the model used had some defects. The chief deficiency of the model is the over-simplified treatment of the carbon structure. This is represented as a distribution of unconnected slit pores having a range of widths (H) chosen to approximately match the experimentally determined pore size distribution, with

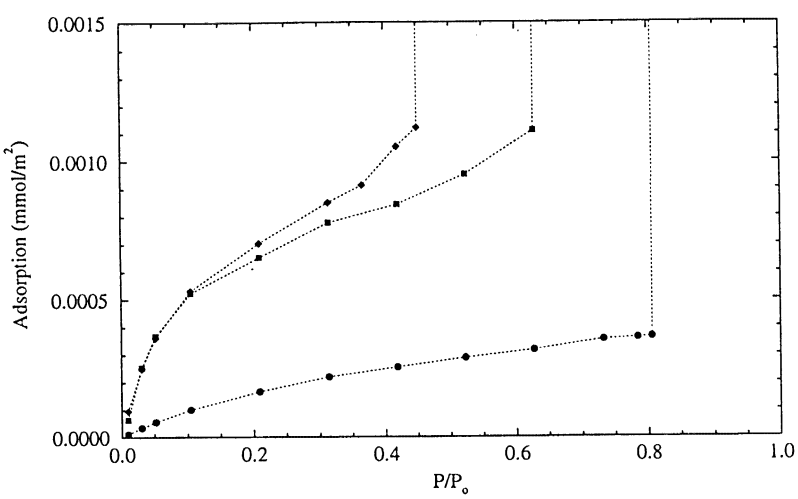

Fig. 20. Effect of surface site density on water adsorption at 298 K in a pore width of 1.69 nm [14]. Three site densities are shown: 0.3 (circles), 0.675 (squares), and 1.2 sites nm^{-2} (diamonds). Reprinted with permission from Ref. [14]copyright 1999, American Chemical Society.

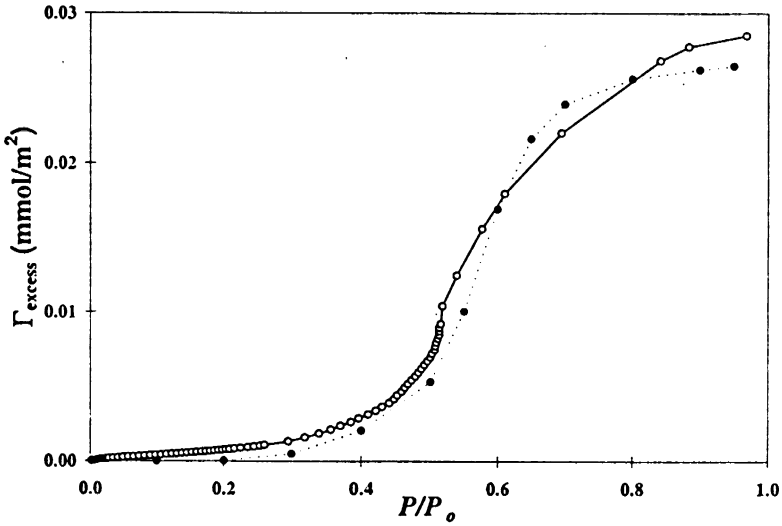

Fig. 21. Comparison of adsorption isotherms for water from experiment (open circles) and simulation (filled circles) at 298 K [14]. Reprinted with permission from Ref. [14] copyright 1999, American Chemical Society.

surfaces composed of graphite basal planes which are decorated with oxygenated sites. Such a model does not allow for effects due to the edges of the carbon microcrystals, nor for the finite size of these or irregular ordering of neighboring crystals. Edge defects are believed to be important in water adsorption, since the oxygenated groups are located at the edge of the microcrystals. In addition, the intermolecular potentials used for both water and water–site interactions neglected long-range interactions and polarizability effects.

Recently, the adsorption behavior of water vapor–methane mixtures in activated carbon pores was simulated by Muller and coworkers [131]. Further refinements of their original model included a more physically realistic placement of the surface sites. They found that the relative adsorption of the two species is strongly dependent on the surface site density. For slit pore width $H =$ 1.0 nm, the adsorption selectivity of methane decreases dramatically as site density increases, where an inversion of selectivity (i.e. water becomes preferentially adsorbed) occurs at a modest site density $n \sim 0.04$ sites nm^{-2}. The crossover from preferential adsorption of methane to water is illustrated in Fig. 22. Snapshots of equilibrium configurations in a pore width $H = 1$ nm with site densities $n = 0.5$ and 1.75 sites nm^{-2} at 300 K are shown. The strong adsorption of water, and consequent exclusion of other organic components, may explain the large reduction in adsorption capacity due to the presence of humidity in feed gas streams that is frequently observed [1,3]. Water clusters formed may effectively block whole pores, diminishing the overall effective surface area that can affect equilibrium as well as diffusion behavior

5.2. More realistic models

The simulation of the adsorption of water in a more realistic carbon structure has recently been carried out [189]. Water molecules are modeled using the fixed-point-charge water model of Errington and Panagiotopoulos [89] described in Section 4.2. The RMC technique described in Section 4.1 was used to generate a realistic model of microporous carbon pore morphologies composed of rigid, carbon basal plates [84]. Arrangements of the carbon plates were driven by a systematic refinement of simulated C–C radial distribution functions to match experiment. Surface sites were placed randomly on the edges of the microcrystals in these structures. The adsorp-

tion of water on activated (surface oxygen sites, =O) and non-activated (graphitic) carbons prepared in this fashion has been investigated using the grand canonical Monte Carlo simulation method at 300 K.

Carbon–water interaction parameters were adjusted to correspond to potentials developed by McCallum et al. [14], who adjusted the dispersion interaction parameters to fit very low-pressure adsorption data (in the pressure region where fluid–fluid interactions are negligible) for an experimental activated carbon that was well characterized. We model the surface oxygen site (=O) as a single Lennard-Jones (LJ) sphere with a point charge fixed at its center. The LJ energy and size parameters are taken from the OPLS format (see, e.g. Ref. [190]) to be $\varepsilon/k = 105.76$ and $\sigma = 0.296$ nm, respectively. The C=O bond length was taken as 0.1214 nm. Finally, the point charge is $q = -0.37e$, which was derived from the quantum chemical electrostatic potential [191]. Electrostatic interactions were estimated using Ewald summation. A spherical cutoff of $3.9\sigma_w$ was applied without long-range corrections. Cubic simulation cells with length either 5.0 nm (carbon structure porosity = 0.485) or 10.0 nm (carbon structure porosity = 0.579) were used.

The adsorption behavior was found to be strongly dependent on the presence of active sites, with no appreciable adsorption in the graphitic carbon until the pressure is very close to the bulk saturation point. Additionally, water adsorption is found to increase as the active site density increases. The adsorption isotherms at 300 K for

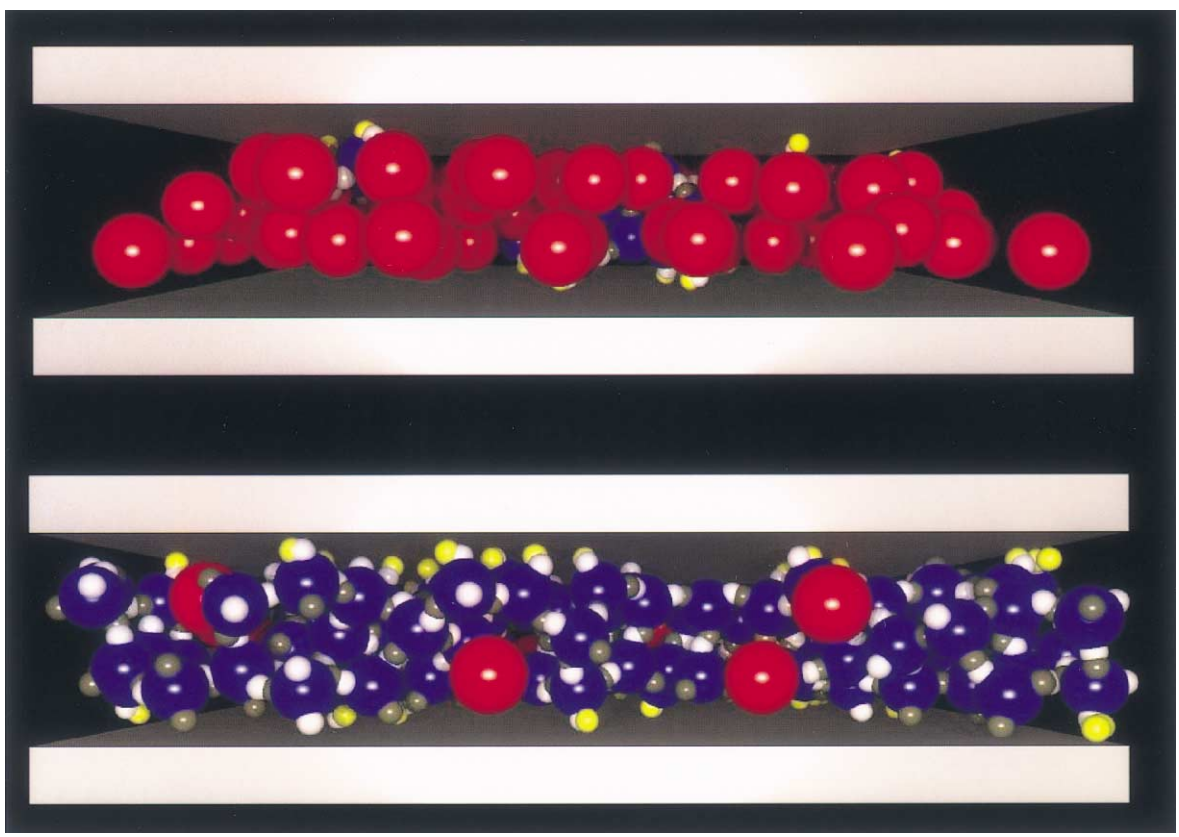

Fig. 22. Snapshots of equilibrium configurations for the adsorption of methane (red spheres) and water (blue spheres) in a pore width $H = 1$ nm with site densities $n = 0.5$ sites nm^{-2} (top) and $n = 1.75$ sites nm^{-2} (bottom) at 300 K. Yellow spheres represent activated sites on the surface of the pore; white and green spheres are the hydrogen and lone pair electron square well sites on the water molecules, respectively. Reprinted with permission from Ref. [131] copyright 2000, American Chemical Society.

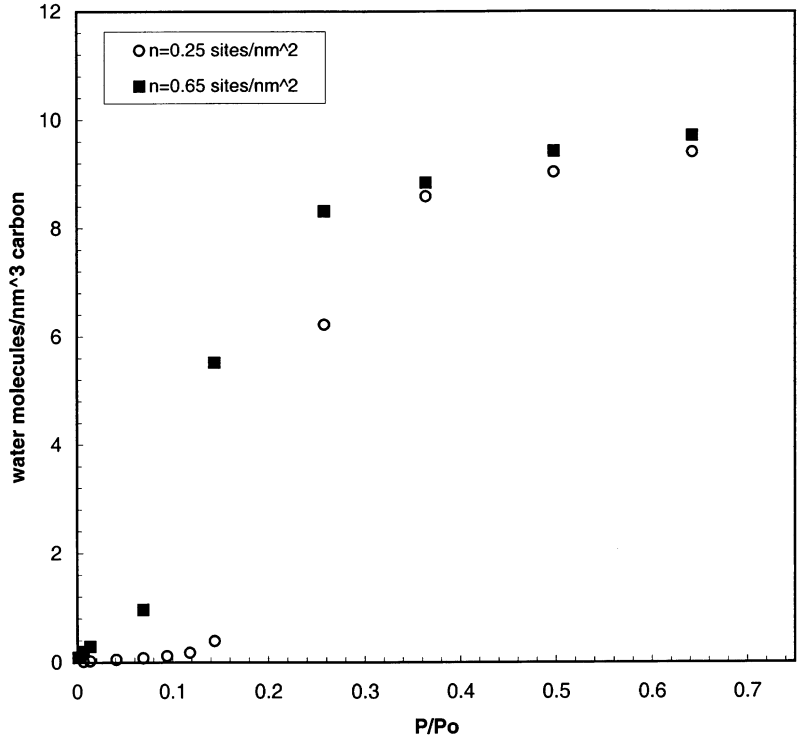

Fig. 23. Adsorption isotherms for water in a realistic activated carbon structure at 300 K. Two site densities, 0.25 (circles) and 0.65 (squares) sites nm^{-2}, are shown.

graphitic carbon agree qualitatively with experimental data for graphitic carbons [3,184] although experimentally the onset of significant water uptake and capillary condensation may occur at lower pressures than in the simulations. This difference can be attributed to structural heterogeneity (e.g. non-aromatic rings of carbon atoms or heteroatoms that induce cross-linking of carbon plates) in actual carbons that are not present in our simplified representation of aromatic carbon plates. Such heterogeneity in actual carbon samples provides additional adsorption sites for the water molecules.

The adsorption behavior of water adsorbed in our activated microporous carbon model is shown in Fig. 23 for activated site densities, $n =$ 0.25 and 0.65 sites nm^{-2}. At low pressures, uptake of water occurs via the bonding of isolated water molecules to the oxygenated surface sites. This stage is followed by a buildup of water clusters around those sites. For the $n = 0.25$ sites nm^{-2} isotherm, when all sites are occupied by water clusters little further uptake occurs as the pressure increases. This is attributed to the sites (and their resident water clusters) being located far from each other so that the bridging of proximal water clusters is unlikely. At the higher site density, continuous uptake occurs as the pressure increases. Water molecules search for locations where they can either bond to several pre-adsorbed water molecules or to a water molecule and a surface site simultaneously — a mechanism recently termed *cooperative bonding* by Muller et al. [13]. A snapshot of a configuration of water adsorbed at high relative-pressure in the carbon sample for $n = 0.65$ sites nm^{-2} is shown in Fig. 24. It should be noted that simulations for different random placement of the active sites found no significant changes in the adsorption behavior.

6. Conclusions and future outlook

Activated carbons can be found throughout the chemical, oil and gas, food, and pharmaceutical industries for purification and separation technologies. They play a central role in many pollution abatement processes — being the most widely used of the common adsorbents. Water purification, as well as the removal of pollutants from gas streams, rely on adsorbent beds of activated carbons. A central need in all of these applications are reliable methods for characterizing carbons. Over the next 5–10 years, with the continual increase in computer power that is anticipated, it should be possible to generate realistic models for carbons having a wide range of pore sizes, porosities, and surface chemistry. Software could then match experimental data on real activated carbons to the model materials contained in a data bank, thus providing a much more sophisticated and complete characterization.

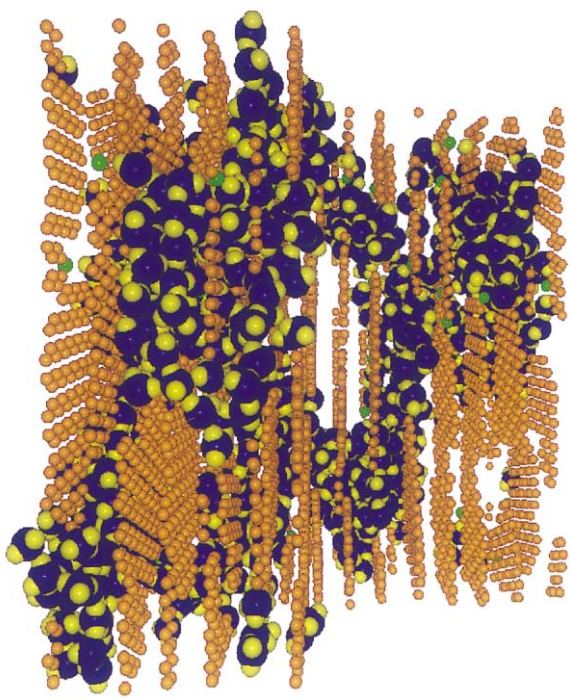

Fig. 24. Snapshot of water adsorption in activated carbon model (site density is 0.65 sites nm^{-2}) at high P/P_0. Orange, green, blue, and yellow spheres represent carbon atoms, activated sites, water molecules, and hydrogen atoms, respectively. For visual clarity, the size of all spheres has been reduced and one-quarter of the simulation box at the right front edge has been removed.

The presence of water in activated carbons has a large effect on the performance of industrial adsorbers, often reducing their useful lifetime by as much as 50%. It is obvious from this review that a thorough molecular-level understanding of the behavior of water in activated carbons is lacking. Gaining a comprehensive understanding by experiment alone has not been successful thus far because of the difficulty of preparing well-characterized carbon structures. Molecular simulation offers the possibility of studying many phenomena exclusively and systematically for precisely defined model materials. Moreover, complementary experimental and simulation studies such as those described in Section 5, appear most promising in understanding the mechanism of water adsorbed in activated carbons.

Acknowledgements

We are grateful to Erich Muller for helpful comments. We thank the Department of Energy for support of this work through grant # DE-FG02-98ER14847. J.K.B and K.T.T thank NSF for support through a NSF-CISE Postdoctoral Fellowship (grant # ACI-9896106). Supercomputer time was provided under a NSF/NRAC grant (# MCA93S011).

References

[1] R. Gong, T.C. Keener, J. Air Waste Manage. Assoc. 43 (1993) 864.
[2] V. Bourdin, P. Grenier, A. Malka-Edery, Fundamentals of Adsorption; Proceedings of the Sixth Conference on Fundamentals of Adsorption, presqu'ile de Giens, France, 24–26 May 1998, Elsevier, Paris, 1998 (p. 1167).
[3] S.J. Gregg, K.S. Sing, Adsorption, Surface Area and Porosity, 2nd ed., Academic Press, New York, 1982.
[4] M.M. Dubinin, Carbon 18 (1980) 355.
[5] M.M. Dubinin, V.V. Serpinsky, Carbon 19 (1981) 402.
[6] R.L. D'Arcy, I.C. Watt, Trans. Faraday Soc. 66 (1970) 1236.
[7] M.J.B. Evans, Carbon 25 (1987) 81.
[8] O. Talu, F. Meunier, AIChE J. 42 (1996) 809.

[9] T. Iiyama, K. Nishikawa, T. Otowa, K. Kaneko, J. Phys. Chem. 99 (1995) 10 075.
[10] Y. Hanzawa, K. Kaneko, Langmuir 13 (1997) 5802.
[11] F. Stoeckli, L. Currit, A. Laederach, T.A. Centeno, J. Chem. Soc. Faraday Trans. 90 (1994) 3689.
[12] I.I. Salame, T.J. Bandosz, Langmuir 15 (1999) 587.
[13] E.A. Muller, L.F. Rull, L.F. Vega, K.E. Gubbins, J. Phys. Chem. 100 (1996) 1189.
[14] C.L McCallum, T.J. Bandosz, S.C. McGrother, E.A. Muller, K.E. Gubbins, Langmuir 15 (1999) 533.
[15] A.J. Groszek, C. Aharoni, Langmuir 15 (1999) 5956.
[16] P. Lodewyckx, E.F. Vansant, Carbon 37 (1999) 1647.
[17] F. Rodriguez-Reinoso, M. Molina-Sabio, M.A. Munecas, J. Phys. Chem. 96 (1992) 2707.
[18] R. Tsunoda, J. Colloid Interface Sci. 218 (1999) 269.
[19] T.J. Bandosz, J. Jagiello, J.A. Schwarz, A. Krzyzanowski, Langmuir 12 (1996) 6480.
[20] B. Buczek, T. Grzybek, A. Bernasik, in: M.D. LeVan (Ed.), Proceedings of the Fifth International Conference on Fundamentals of Adsorption, Kluwer, Boston, 1996, p. 109.
[21] J. Choma, W. Burakiewicz-Mortka, M. Jaroniec, Z. Li, J. Klinik, J. Colloid Interface Sci. 214 (1999) 438.
[22] A.W. Harding, N.J. Foley, P.R. Norman, D.C. Francis, K.M. Thomas, Langmuir 14 (1998) 3858.
[23] A.M. Youssef, T.M. Ghazy, Th. El-Nabarawy, Carbon 20 (1982) 113.
[24] R.H. Bradley, B. Rand, Carbon 29 (1991) 1165.
[25] R.H. Bradley, B. Rand, Carbon 31 (1993) 269.
[26] E. Biron, M.J.B. Evans, Carbon 36 (1998) 1191.
[27] H.F. Stoeckli, F. Kraehenbuehl, D. Morel, Carbon 21 (1983) 589.
[28] W.H. Lee, P.J. Reucroft, Carbon 37 (1999) 7.
[29] N.N. Avgul, O.M. Dzhigit, A.V. Kiselev, K.D. Shcherbakova, Dokl. AN SSSR 92 (1953) 105.
[30] N.N. Avgul, O.M. Dzhigit, A.V. Kiselev, K.D. Shcherbakova, Dokl. AN SSSR 101 (1955) 285.
[31] N.N. Avgul, A.V. Kiselev, in: P.L. Walker Jr. (Ed.), Chemistry and Physics of Carbon, vol. 6, Marcel Dekker, New York, 1970, p. 1.
[32] F. Carrasco-Marin, A. Mueden, T.A. Centeno, F. Stoeckli, C. Moreno-Castilla, Chem. Soc. Faraday Trans. 93 (1997) 2211.
[33] T.J. Bandosz, B. Buczek, T. Grzybek, J. Jagiello, Fuel 76 (1997) 1409.
[34] S.S. Barton, M.J.B. Evans, J.A.F. MacDonald, Carbon 29 (1991) 1099.
[35] S.S. Barton, M.J.B. Evans, J.A.F. MacDonald, Carbon 36 (1998) 969.
[36] S.S. Barton, M.J.B. Evans, J. Holland, J.E. Koresh, Carbon 22 (1984) 265.
[37] I.I. Salame, T.J. Bandosz, J. Colloid Interface Sci. 210 (1999) 367.
[38] I.I. Salame, A. Bagreev, T.J. Bandosz, J. Phys. Chem. 103 (1999) 3877.
[39] N.M. Hassan, T.K. Ghosh, A.L. Hines, S.K. Loyalka, Carbon 29 (1991) 681.
[40] R.Sh. Vartapetyan, A.M. Voloshchuk, A.A. Isirikyan, N.S. Polyakov, Y.I. Tarasevich, Colloids Surf. A 101 (1995) 227.
[41] H. Naono, M. Hakuman, M. Shimoda, K. Nakai, S. Kondo, J. Colloid Interface Sci. 182 (1996) 230.
[42] E.N. Rudisill, J.J. Hacskaylo, M.D. LeVan, Ind. Engng Chem. Res. 31 (1992) 1122.
[43] I.I. Salame, T.J. Bandosz, Langmuir 16 (2000) 5435.
[44] P.B. Balbuena, K.E. Gubbins, Langmuir 9 (1993) 1801.
[45] B.R. Puri, in: P.L. Walker Jr. (Ed.), Chemistry and Physics of Carbons, vol. 6, Marcel Dekker, New York, 1970, p. 191.
[46] H.P. Boehm, Advances in Catalysis, vol. 16, Academic Press, New York, 1966 (p. 179).
[47] C.A. Leon y Leon, L.R. Radovic, in: P.A. Thrower (Ed.), Chemistry and Physics of Carbon, vol. 24, Marcel Dekker, New York, 1992, p. 213.
[48] G. Kortum, W. Vogel, K. Andrussow, Dissociation Constants of Organic Acids in Aqueous Solutions, Butterworth, London, 1961.
[49] E.M. Perdue, J.H. Reuter, R.S. Parrish, Geochim. Cosmochim. Acta. 48 (1984).
[50] C.A. Leon y Leon, J.M. Solar, V. Calemma, L.R. Radovic, Carbon 30 (1992) 797.
[51] V.A. Garten, D.E. Weiss, Rev. Pure Appl. Chem. 7 (1957) 69.
[52] C. Contescu, J. Jagiello, J.A. Schwarz, Langmuir 9 (1993) 1754.
[53] T.J. Bandosz, J. Jagiello, C. Contescu, J.A. Schwarz, Carbon 31 (1993) 1193.
[54] J. Jagiello, Langmuir 10 (1994) 2778.
[55] J. Jagiello, T.J. Bandosz, J.A. Schwarz, Carbon 32 (1994) 1026.
[56] J. Jagiello, T.J. Bandosz, K. Putyera, J.A. Schwarz, J. Colloid Interface Sci. 172 (1995) 341.
[57] A. Contescu, C. Contescu, K. Putyera, J.A. Schwarz, Carbon 35 (1997) 83.
[58] F. Adib, A. Bagreev, T.J. Bandosz, J. Colloid Interface Sci. 214 (1999) 407.
[59] N.R. Laine, F.J. Vasola, P.L. Walker Jr., J. Phys. Chem. 67 (1963) 2030.
[60] E. Papirer, J. Dentzer, S. Li, J.B. Donnet, Carbon 29 (1991) 69.
[61] Y. Otake, R.G. Jenkins, Carbon 31 (1993) 109.
[62] A. Proctor, P.M.A. Sherwood, Carbon 21 (1983) 53.
[63] C. Kozlowski, P.M.A. Sherwood, Carbon 24 (1986) 357.
[64] J.B. Donnet, G. Guilpain, Carbon 27 (1989) 749.
[65] J. Zawadzki, in: P.A. Thrower (Ed.), Chemistry and Physics of Carbon, vol. 21, Marcel Dekker, New York, 1989, p. 180.
[66] F. Rodriguez-Reinoso, M. Molina-Sabio, M.T. Gonzalez, Langmuir 13 (1997) 2354.
[67] F. Rodriguez-Reinoso, M. Molina-Sabio, Adv. Colloid Interface Sci. 76-77 (1998) 271.
[68] D.D. Do, H.D. Do, Carbon 38 (2000) 767.
[69] M.M. Dubinin, V.A. Astakhov, Adv. Chem. Ser. 102 (1970) 69.

[70] D. Nicholson, J. Chem. Soc. Faraday Trans. 92 (1996) 1.
[71] Z. Tan, K.E. Gubbins, J. Phys. Chem. 96 (1992) 845.
[72] S. Jiang, J.A. Zollweg, K.E. Gubbins, J. Phys. Chem. 98 (1994) 5709.
[73] T. Shigeta, J. Yoneya, T. Nitta, Mol. Simul. 16 (1996) 291.
[74] V.Y. Gusev, J.A. O'Brien, Langmuir 14 (1998) 6328.
[75] C. Nguyen, D.D. Do, Langmuir 15 (1999) 3608.
[76] C. Lastoskie, K.E. Gubbins, N. Quirke, J. Phys. Chem. 97 (1993) 4786.
[77] B. McEnaney, T.J. Mays, X. Chen, Fuel 77 (1998) 557.
[78] J. Rodriguez, F. Ruette, J. Laine, Carbon 32 (1994) 1536.
[79] E.I. Segarra, E.D. Glandt, Chem. Engng Sci. 49 (1994) 2953.
[80] R. Eppenga, D. Frenkel, Mol. Phys. 52 (1984) 1303.
[81] J.R Dahn, W. Xing, Y. Gao, Carbon 35 (1997) 825.
[82] N.A. Seaton, S.P. Friedman, J.M.D. MacElroy, B.J. Murphy, Langmuir 13 (1997) 1199.
[83] M.J. Bojan, W.A. Steele, Langmuir 9 (1993) 2569.
[84] K.T. Thomson, K.E. Gubbins, Langmuir 16 (2000) 5761.
[85] R.L. McGreevy, L. Putszai, Mol. Simul. 1 (1988) 359.
[86] R.L. McGreevy, M.A. Rowe, D.A. Keen, K. Clausen, IOP Conf. Ser. 107 (1990) 165.
[87] F.L.B. da Silva, B. Svensson, T. Akesson, B. Jonsson, J. Chem. Phys. 109 (1998) 2624.
[88] K.E. Gubbins, N. Quirke, in: K.E. Gubbins, N. Quirke (Eds.), Molecular Simulations and Industrial Applications, Gordon and Breach, Amsterdam, 1996, pp. 17–25.
[89] J.R. Errington, A.Z. Panagiotopoulos, J. Phys. Chem. 102 (1998) 7470.
[90] K. Kiyohara, K.E. Gubbins, A.Z. Panagiotopoulos, Mol. Phys. 94 (1998) 803.
[91] A.A. Chialvo, P.T. Cummings, Adv. Chem. Phys. 109 (1999) 115.
[92] Y.P. Liu, K. Kim, B.J. Berne, R.A. Friesner, S.W. Rick, J. Chem. Phys. 108 (1998) 4739.
[93] J.D. Bernal, R.H. Fowler, J. Chem. Phys. 110 (1933) 97.
[94] F.H. Stillinger, A. Rahman, J. Chem. Phys. 60 (1974) 1545.
[95] W.L. Jorgensen, J. Chem. Phys. 77 (1982) 4156.
[96] W.L. Jorgensen, J. Chandrasekhar, J.D. Madura, R.W. Impley, M.L. Klein, J. Chem. Phys. 79 (1983) 926.
[97] H.J.C. Berendsen, J.P.M. Postma, W.F. van Gunsteren, J. Hermans, in: B. Pullman (Ed.), Intermolecular Forces, Reidel, Holland, Dordrecht, 1981.
[98] H.J.C. Berendsen, J.R. Grigera, J.R. Straatsma, J. Phys. Chem. 91 (1987) 9269.
[99] G.C. Boulougouris, I.G. Economou, D.N. Theodorou, J. Phys. Chem. B 102 (1998) 1029.
[100] W. Bol, Mol. Phys. 45 (1982) 605.
[101] J. Kolafa, I. Nezbeda, Mol. Phys. 72 (1991) 777.
[102] D. Ghonsagi, W. Chapman, Mol. Phys. 79 (1993) 291.
[103] E.A. Muller, K.E. Gubbins, Ind. Engng Chem. Res. 34 (1995) 3662.
[104] W.L. Jorgensen, J. Am. Chem. Soc. 103 (1981) 335.
[105] I.M. Svishchev, P.G. Kusalik, J. Wang, R.J. Boyd, J. Chem. Phys. 105 (1996) 4742.
[106] L.X. Dang, J. Chem. Phys. 97 (1992) 2659.
[107] F.H. Stillinger, C.W. David, J. Chem. Phys. 69 (1978) 1473.
[108] M. Sprik, M.L. Klein, J. Chem. Phys. 89 (1988) 7556.
[109] J.A.C. Rullmann, P.T. van Duijnen, Mol. Phys. 63 (1988) 451.
[110] P. Ahlstrom, A. Wallquist, S. Engstrom, B. Jonsson, Mol. Phys. 68 (1989) 563.
[111] S. Kuwajima, A. Warshel, J. Phys. Chem. 94 (1990) 460.
[112] S.W. Rick, S.J. Stuart, B.J. Berne, J. Chem. Phys. 101 (1994) 6141.
[113] K. Toukan, A. Rahman, Phys. Rev. B 31 (1985) 2643.
[114] G.C. Lie, E. Clementi, Phys. Rev. A 33 (1986) 2679.
[115] J. Anderson, J.J. Ullo, S. Yip, J. Chem. Phys. 87 (1987) 1726.
[116] S.B. Zhu, S. Singh, G.W. Robinson, J. Chem. Phys. 95 (1991) 2791.
[117] U. Niesar, G. Corongiu, E. Clementi, G.R. Kneller, D.K. Bhattacharya, J. Phys. Chem. 94 (1990) 7949.
[118] A. Famulari, R. Specchio, M. Sironi, M. Raimondi, J. Chem. Phys. 108 (1998) 3296.
[119] A.Z. Panagiotopoulos, J. Phys. Chem. B 112 (2000), 7132.
[120] J. Caldwell, L.X. Dang, P.A. Kollman, J. Am. Chem. Soc. 112 (1990) 9144.
[121] R.D. Mountain, J. Chem. Phys. 103 (1995) 3084.
[122] J.R. Errington, A.Z. Panagiotopoulos (2001), in press.
[123] A.A. Chialvo, P.T. Cummings, Fluid Phase Equilib. 150-151 (1998) 73.
[124] A.A. Chialvo, P.T. Cummings, J.M. Simonson, R.E. Mesmer, H.D. Cochran, Ind. Engng Chem. Res. 37 (1998) 3021.
[125] W.A. Steele, The Interaction of Gases with Solid Surfaces, Pergamon, Oxford, 1974.
[126] M. Maddox, D.E. Ulberg, K.E. Gubbins, Fluid Phase Equilib. 104 (1995) 145.
[127] D. Wang, A. Sakoda, M. Suzuki, Adsorption 5 (1999) 97.
[128] E.A. Muller, K.E. Gubbins, Ind. Engng Chem. Res. 34 (1995) 3662.
[129] P.A. Gordon, E.D. Glandt, Langmuir 13 (1997) 4659.
[130] S.S. Barton, M.J.B. Evans, J. MacDonald, Langmuir 10 (1994) 4250.
[131] E.A. Muller, F.R. Hung, K.E. Gubbins, Langmuir 16 (2000) 5418.
[132] A.V. Vernov, W.A. Steele, Langmuir 8 (1992) 155.
[133] F.Y. Hansen, L.W. Bruch, S.E. Roosevelt, Phys. Rev. B 45 (1992) 11 238.
[134] F.Y. Hansen, L.W. Bruch, H. Taub, Phys. Rev. B 52 (1995) 8515.
[135] D.B. Whitehouse, A.D. Buckingham, J. Chem. Soc. Faraday Trans. 2 89 (1993) 1909.
[136] L.W. Bruch, M.W. Cole, E. Zaremba, Physical Adsorption: Forces and Phenomena, Oxford University Press, Oxford, 1997 (chap. 2).

[137] C.G. Gray, K.E. Gubbins, Theory of Molecular Fluids, Clarendon Press, Oxford, 1984 (section 2.10).
[138] D. Nicholson, Surf. Sci. 181 (1987) L189.
[139] D. Nicholson, in: A.B. Mersmann, S.E. Scholl (Eds.), Fundamentals of Adsorption, Engineering Foundation, New York, 1991, pp. 3–12.
[140] V. Lachet, A. Boutin, B. Tavitian, A.H. Fuchs, J. Phys. Chem. B 102 (1998) 9224.
[141] D. Nicholson, R.J.M. Pellenq, Adv. Colloid Interface Sci. 76–77 (1998) 179.
[142] R.J.M. Pellenq, D. Nicholson, Mol. Phys. 95 (1998) 549.
[143] R. Klein, L.W. Bruch, M.W. Cole, Surf. Sci. 173 (1986) 555.
[144] R.C. Bansal, J. Donnet, in: J. Donnet, R.C. Bansal, M. Wang (Eds.), Carbon Black, Marcel Dekker, New York, 1993.
[145] G.E. Norman, V.S. Filinov, High Temp. (USSR) 7 (1969) 216.
[146] M.P. Allen, D.J. Tildesley, Computer Simulation of Liquids, Clarendon, Oxford, 1987.
[147] D. Frenkel, B. Smit, Understanding Molecular Simulation, Academic Press, New York, 1996.
[148] S.C. McGrother, K.E. Gubbins, Mol. Phys. 97 (1999) 955.
[149] B.K. Peterson, K.E. Gubbins, Mol. Phys. 62 (1987) 215.
[150] B.K. Peterson, K.E. Gubbins, G.S. Heffelfinger, U. Marini Bettolo Marconi, F. van Swol, J. Chem. Phys. 88 (1988) 6487.
[151] K.S. Page, P.A. Monson, Phys. Rev. E 54 (1996) R29.
[152] K.S. Page, P.A. Monson, Phys. Rev. E 54 (1996) 6557.
[153] A.Z. Panagiotopoulos, Mol. Phys. 61 (1987) 813.
[154] A.Z. Panagiotopoulos, N. Quirke, M. Stapleton, D.J. Tildesley, Mol. Phys. 63 (1988) 527.
[155] S. Jiang, K.E. Gubbins, Mol. Phys. 86 (1995) 599.
[156] A.Z. Panagiotopoulos, Mol. Phys. 62 (1987) 701.
[157] W.T. Gozdz, K.E. Gubbins, A.Z. Panagiotopoulos, Mol. Phys. 84 (1995) 825.
[158] P.A. Gordon, E.D. Glandt, Phys. Rev. E 105 (1996) 4257.
[159] J.K. Brennan, W. Dong, J. Chem. Phys., submitted for publication.
[160] J.K. Brennan, W. Dong, Phys. Rev. Lett., submitted for publication.
[161] D.A. Kofke, E.D. Glandt, Mol. Phys. 64 (1988) 1105.
[162] L.D. Gelb, K.E. Gubbins, Phys. Rev. E 56 (1997) 3185.
[163] L.D. Gelb, K.E. Gubbins, Physica A 244 (1997) 112.
[164] C.H. Bennett, J. Comput. Phys. 22 (1976) 245.
[165] I.R. McDonald, K. Singer, J. Chem. Phys. 47 (1967) 4766.
[166] A.M. Ferrenberg, D.P. Landau, R.H. Swendsen, Phys. Rev. E 51 (1995) 5092.
[167] A.M. Ferrenberg, R.H. Swendsen, Phys. Rev. Lett. 61 (1988) 2635.
[168] A.M. Ferrenberg, R.H. Swendsen, Phys. Rev. Lett. 63 (1989) 1195.
[169] B.A. Berg, T. Neuhaus, Phys. Rev. B 267 (1991) 249.
[170] G. Orkoulas, A.Z. Panagiotopoulos, J. Chem. Phys. 110 (1999) 1581.
[171] G. Orkoulas, A.Z. Panagiotopoulos, J. Chem. Phys. 110 (1999) 1590.
[172] R. Radhakrishnan, K.E. Gubbins, Mol. Phys. 96 (1999) 1249.
[173] R.M. Lynden-Bell, J.S. van Duijneveldt, D. Frenkel, Mol. Phys. 80 (1993) 801.
[174] P. Keblinski, W.-J. Ma, A. Maritan, J. Koplik, J.R. Banavar, Phys. Rev. E 47 (1993) R2265.
[175] Z. Zhang, A. Chakrabarti, Phys. Rev. B 52 (1995) 2736.
[176] L.D. Gelb, K.E. Gubbins, Phys. Rev. E 55 (1997) R1290.
[177] Z. Zhang, A. Chakrabarti, Phys. Rev. E 50 (1994) R4290.
[178] B. Strickland, G. Leptoukh, C. Roland, J. Phys. A: Math. Gen. 28 (1995) L403.
[179] D. Nicholson, N.G. Parsonage, Computer Simulation and the Statistical Mechanics of Adsorption, Academic Press, London, 1982.
[180] V.Y. Antonchenko, A.S. Davidov, V. Ilyin, Physics of Water, Naukova Dumka, Kiev, 1991.
[181] D.E. Ulberg, K.E. Gubbins, Mol. Simul. 13 (1994) 205.
[182] D.E. Ulberg, K.E. Gubbins, Mol. Phys. 84 (1995) 1139.
[183] M. Maddox, D.E. Ulberg, K.E. Gubbins, Fluid Phase Equilib. 104 (1995) 145.
[184] F. Rouquerol, J. Rouquerol, K.S. Sing, Adsorption by Powders and Porous Solids, Academic Press, London, 1999, p. 1999.
[185] E.A. Muller, K.E. Gubbins, Carbon 36 (1998) 1433.
[186] J.M. Briggs, T.B. Nguyen, W.L. Jorgensen, J. Phys. Chem. 95 (1991) 3315.
[187] T.J. Bandosz, F.J. Blas, K.E. Gubbins, C.L. McCallum, S.C. McGrother, S.L. Sowers, L.F. Vega, Proc. Mater. Res. Soc. 497 (1998) 231.
[188] T.J. Bandosz, K.E. Gubbins, C.L. McCallum, S.C. McGrother, E.A. Muller, S.L. Sowers, Fundamentals of Adsorption; Proceedings of the Sixth Conference on Fundamentals of Adsorption, presqu'ile de Giens, France, 24–26 May 1998, Elsevier, Paris, 1998 (p. 213).
[189] J.K. Brennan, K.T. Thomson, K.E. Gubbins, submitted for publication.
[190] W.L. Jorgensen, C.J. Swenson, J. Am. Chem. Soc. 107 (1985) 569.
[191] E. Sigfridsson, U. Ryde, J. Comput. Chem. 19 (1998) 377.
[192] A.K. Soper, J. Turner, Int. J. Mod. Phys. B 7 (1993) 3049.